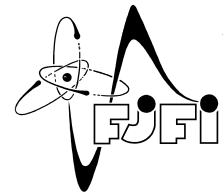




CZECH TECHNICAL UNIVERSITY IN PRAGUE
Faculty of Nuclear Sciences and Physical
Engineering

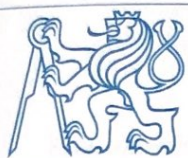


Characterization of neutron field in graphite insertion in LR-0 core

Charakterizace neutronového pole v grafitové vložné zóně v reaktoru LR-0

Master's Degree Project

Author: Bc. Mikita Sobaleu
Supervisor: Ing. Michal Košťál, Ph.D.
Consultant: Ing. Evžen Losa, Ph.D.
Academic year: 2019/2020



ZADÁNÍ DIPLOMOVÉ PRÁCE

Student: **Bc. Mikita Sobaleu**

Studijní program: Aplikace přírodních věd

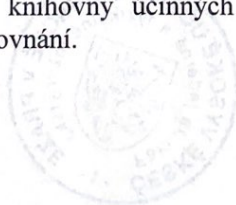
Obor: Jaderné inženýrství

Název práce česky: **Charakterizace neutronového pole v grafitové vložné zóně v reaktoru LR-0**

Název práce anglicky: Characterization of neutron field in graphite insertion in LR-0 core

Pokyny pro vypracování:

1. Proveďte rešerši integrálních experimentů používaných pro validace dozimetrických účinných průřezů materiálů využívaných v jaderných technologiích. Prozkoumejte možnosti filtrování neutronového pole a jeho využití v testování účinných průřezů v různých energetických oblastech.
2. Seznamte se s metodikou hodnocení reakčních rychlostí z aktivačních experimentů při použití nebudových terčů ve speciální zóně v reaktoru LR-0.
3. Seznamte se s metodikou účinnostní kalibrace prostřednictvím matematického modelu HPGe v laboratořích LR-0. S pomocí Vámi vypočtených účinností vyhodnoťte experimentální reakční rychlosti aktivačních detektorů ve speciální zóně v reaktoru LR-0.
4. Seznamte se s benchmarkovým modelem speciální grafitové vložné zóny na kritičnost sestaveným v kódu MCNP a upravte jej pro potřeby výpočtu reakčních rychlostí vybraných dozimetrických reakcí v použitých aktivačních detektorech.
5. S výsledným modelem proveďte výpočet reakčních rychlostí v použitých aktivačních detektorech a porovnejte s experimentálními daty. Porovnejte soulad experimentu se simulacemi využívajícími různé knihovny účinných průřezů dozimetrických reakcí. Proveďte odhad nejistot pro toto srovnání.



Doporučená literatura:

- [1] Reuss, P., Neutron Physic, ISBN 2759800415, 9782759800414, EDP Sciences, 2008
- [2] Trkov, A. et al., IRDFF-II: A New Neutron Metrology Library, Nuclear Data Sheets, in preparation
- [3] Radulovic, V. et al., Integral Data in Nuclear Data Evaluation, Summary Report INDC(NDS)-0746, IAEA Vienna, 2018
- [4] Dryak, P, Kovar, P., Experimental and MC determination of HPGe detector efficiency in the 40–2754 keV energy range for measuring point source geometry with the source-to-detector distance of 25 cm, Appl. Rad. Isot., 64, (2006), pp. 1346–1349
- [5] Košťál, M. et al., Validation of zirconium isotopes (n, g) and (n, 2n) cross sections in a comprehensive LR-0 reactor operative parameters set, Applied Radiation and Isotopes, 128, (2017), pp. 92–100
- [6] Košťál, M. et al., VVER-1000 Low Enriched U(3.6 wt.% U235)O2 Fuel Assemblies in Light Water with Seven Void, Silicon Dioxide or Graphite Modules in Center, 2020, OECD-NEA, LR(0)-VVER-RESR-005, benchmark z databáze projektu IRPhE, v přípravě

Jméno a pracoviště vedoucího práce: **Ing. Michal Košťál, Ph.D.**
Centrum výzkumu Řež

Jméno a pracoviště konzultanta: **Ing. Evžen Losa, Ph.D.**
KJR FJFI ČVUT v Praze

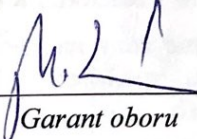
Datum zadání diplomové práce: 17. 10. 2019

Datum odevzdání diplomové práce: 4. 5. 2020

Doba platnosti zadání je dva roky od data zadání.

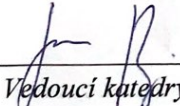
V Praze dne 17. 10. 2019

doc. Ing. Martin Kropík, CSc.



Garant oboru

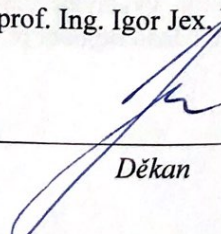
Ing. Jan Rataj, Ph.D.



Vedoucí katedry



prof. Ing. Igor Jex, DrSc.



Děkan

Acknowledgment:

I would like to thank my supervisor Ing. Michal Košťál, Ph.D. for his expert guidance, for help and advice on the work. My thanks also belong to my family for support.

Author's declaration:

I declare that this Master's Degree Project is entirely my own work and I have listed all the used sources in the bibliography.

Prague, June 15, 2020

Mikita Sobaleu

Název práce:

Charakterizace neutronového pole v grafitové vložné zóně v reaktoru LR-0

Autor: Mikita Sobaleu

Obor: Jaderné inženýrství

Druh práce: Diplomová práce

Vedoucí práce: Ing. Michal Košťál, Ph.D., Centrum výkumu Řež

Konzultant: Ing. Evžen Losa, Ph.D., Katedra jaderných reaktorů, FJFI, ČVUT v Praze

Abstrakt: Diplomová práce věnuje charakterizaci neutronového pole ve speciální grafitové vložné zóně reaktoru LR-0. V důsledku použití grafitu, referenční neutronové spektrum LR-0 bylo termalizováno. Předpokládalo se, že by nové spektrum měl zvýšený podíl epithermálních neutronů, což se hodí pro testování účinných průřezů v oblasti epithermálních energií. Byl připraven MCNP model grafitové zóny na základě MCNP modelu referenční zóny. Byl ukázán vliv neutronových filtrů na citlivost reakcí v různých energetických oblastech. Charakterizace neutronového pole grafitové aktivní zóny byla provedena pomocí vyhodnocení reakčních rychlostí dobře validovaných reakcí. Výsledky ukázaly, že připravený MCNP model dobře charakterizuje získané neutronové pole. Kromě toho, byla provedena validace dalších reakčních rychlostí dozimetrických reakcí v získaném neutronovém spektru.

Klíčová slova: charakterizace neutronového pole, dozimetrické reakce, grafitová vložná zóna, integrální experimenty, LR-0, vyhodnocení reakčních rychlostí

Title:

Characterization of neutron field in graphite insertion in LR-0 core

Author: Mikita Sobaleu

Abstract: The present Master's thesis seeks to characterize a neutron field in a special LR-0 reactor core. As a result of using graphite, the reference LR-0 neutron spectrum got thermalized. The new spectrum is supposed to increase an epithermal neutrons share to validate cross-sections in the epithermal energy region. The MCNP model of the graphite core was prepared using the reference core MCNP model. The impact of neutron filters on reactions sensitivity in different energy regions was illustrated. The characterization of the graphite core neutron spectrum was made by means of reaction rates evaluation of well-validated reactions. The results showed that MCNP model characterizes the neutron field well. Moreover, validation of other reaction rates of dosimetric reactions in the obtained neutron spectrum was made.

Key words: characterization of neutron field, dosimetric reactions, graphite insertion, integral experiments, LR-0, reaction rates evaluation

Contents

Introduction	11
1 Integral Experiments	13
1.1 Criteria for Nuclear Data Validation	14
1.2 Validation of Neutron cross-sections	15
1.3 Validation Integral Experiments in RC Řež	18
1.4 Neutron Filters in Validation	21
2 Evaluation of Reaction Rates on LR-0	25
2.1 Activation experiments	25
2.2 Experimental Reaction Rate	26
2.2.1 Relative Portion of Saturated Activity	27
2.2.2 Dead Time Correction	28
2.2.3 Coincidence Summing Effect Correction	28
2.2.4 Reaction Rate Normalization	29
2.2.5 Self-shielding Correction	30
2.3 Evaluation of Reaction Rates	31
2.3.1 Uncertainties	32
3 Efficiency Calibration of the HPGe Detector on LR-0	34
3.1 Characterization of the HPGe Detector on LR-0	35
3.1.1 Radiography	36
3.1.2 Dead Layer Thickness	37
3.2 Monte Carlo Model of the HPGe Detector on LR-0	40
4 Experimental Part	42
4.1 Description of Experiment	42
4.2 Monte Carlo Model of LR-0	46

4.2.1	Monte Carlo Computational Codes	46
4.2.2	Calculation MCNP Model of LR-0	46
4.3	Results and Uncertainties	48
4.3.1	Uncertainties	55
Conclusion		57
A Comparison of Reaction Rates		64

List of Figures

1.1	Cross-section for reactions $^{58}\text{Fe}(n,\gamma)^{59}\text{Fe}$ in different nuclear data libraries. [11]	17
1.2	LR-0 scheme. [30]	20
1.3	The view inside the reference core of LR-0 reactor (left) and its radial plot (right). [18]	20
1.4	Unfiltered and filtered neutron fields in the special graphite core of LR-0 reactor.	22
1.5	Reaction rate share for $^{63}\text{Cu}(n,\gamma)$ in different neutron spectra.	22
1.6	Reaction rate share for $^{54}\text{Fe}(n,p)$ in different neutron spectra.	23
1.7	Reaction rate share for $^{58}\text{Fe}(n,\gamma)$ in different neutron spectra.	23
1.8	Reaction rate share for $^{181}\text{Ta}(n,\gamma)$ in different neutron spectra.	24
1.9	Reaction rate share for $^{23}\text{Na}(n,\gamma)$ in different neutron spectra.	24
2.1	Production of radioisotopes on the time of irradiation. [1]	26
3.1	Scheme of the p-type HPGe detector: side view (left) [21], top view (right) [12].	36
3.2	Picture of the HPGe detector radiogram (p-type Ortec GEM 35). [1]	37
3.3	General character of inner peak efficiency for n- and p-type HPGe detectors. Efficiency is decreased by the dead layer at low energy region (n-type has thinner dead layer). [12]	39
3.4	The photo (left) and the scheme (right) of the lead collimator for the dead layer thickness measurement.[1]	39
3.5	The dead layer measurement scheme (all distances between measured points on black lines are 6 mm). [1]	40
3.6	3D graph of front dead layer thicknesses. [1]	40
3.7	MCNP model of the HPGe detector with activated material in EG3 capsule. [21]	41
4.1	Relative power during activation.	44
4.2	Construction of a graphite block. [35]	44
4.3	Overhead view at LR-0 reactor core with seven graphite blocks in the middle. The fuel loading cartogram to the right.	45

4.4	Picture and scheme of the holders with activation samples.	45
4.5	Special graphite core of LR-0 reactor with holder in the centre cavity in MCNP model.	48
4.6	Calculated neutron spectra in two LR-0 cores.	52
4.7	Reaction rates evaluation for $^{63}\text{Cu}(n,\gamma)^{64}\text{Cu}$	52
4.8	Reaction rates evaluation for $^{54}\text{Fe}(n,p)^{54}\text{Mn}$	53
4.9	Reaction rates evaluation for $^{58}\text{Fe}(n,\gamma)^{59}\text{Fe}$	53
4.10	Reaction rates evaluation for $^{64}\text{Zn}(n,\gamma)^{65}\text{Zn}$	54
4.11	Reaction rates evaluation for $^{181}\text{Ta}(n,\gamma)^{182}\text{Ta}$	54
4.12	Reaction rates evaluation for $^{23}\text{Na}(n,\gamma)^{24}\text{Na}$	55

List of Tables

1.1	Basic characteristics of LR-0. [30]	19
3.1	Detector parameters obtained from radiogram. [1]	36
4.1	Parameters of scaling factors for two experiments.	50
4.2	Measurement parameters of the activation samples.	51
4.3	Self-shielding correction factors for two LR-0 cores.	51
4.4	Experimental reaction rates (normalized and corrected).	51
4.5	Uncertainties common for all the activation samples.	56
4.6	Statistical errors of the peaks measurements.	56
A.1	Comparison of reaction rates for $^{63}\text{Cu}(n,\gamma)^{64}\text{Cu}$.	64
A.2	Comparison of reaction rates for $^{64}\text{Zn}(n,\gamma)^{65}\text{Zn}$.	64
A.3	Comparison of reaction rates for $^{54}\text{Fe}(n,p)^{54}\text{Mn}$.	65
A.4	Comparison of reaction rates for $^{58}\text{Fe}(n,\gamma)^{59}\text{Fe}$.	65
A.5	Comparison of reaction rates for $^{181}\text{Ta}(n,\gamma)^{182}\text{Ta}$.	66
A.6	Comparison of reaction rates for $^{23}\text{Na}(n,\gamma)^{24}\text{Na}$.	66

Introduction

LR-0 reactor is a versatile tool in reactor physics research. Reactor construction implies experiments with VVER-1000 (or VVER-440) fuel assemblies to study characteristics of reactor dosimetry, criticality parameters, neutron transport, and core power distribution. The modular design of reactor supporting structures allows creating a wide range of various core sizes and geometries.

The neutron field of one of special cores LR-0 is defined as the reference benchmark field. Reference benchmark fields are not so well-described as standard fields but considered as reproducible and permanent, which makes it acceptable as a measurement reference by a community of users. The IAEA community acknowledged the reference LR-0 neutron field. The well-validated MCNP model of the reference core proved that its neutron spectrum is indistinguishable from standard ^{235}U fission spectrum above 6 MeV [16].

A large number of dosimetric cross-sections were validated in the reference spectrum. As a result, the outcomes were included in the new library of dosimetric cross-sections – IRDFF-2.0 [36]. However, there is still a matter to validate these cross-sections in other regions of the spectrum, especially in epithermal. Moderators and absorbers as neutron filters can be applied to alter the neutron spectrum. LR-0 core was changed to increase an epithermal neutrons share. For this purpose, the graphite insertion was placed in the center cavity among fuel assemblies. The option with 7 graphite blocks was selected to provide sufficient thermalization of the reference neutron spectrum, while the neutron flux was not low to keep acceptable irradiation conditions. Graphite has a well-described cross-section due to the wide experience in the energetic nuclear reactors (Magnox, RBMK, etc.) and current interest in generation IV reactors designs such as VHTR and MSR. An example of a generation IV MSR reactor can be Czech small modular reactor Energy Well [29]. Validation of the graphite cross-section was furthermore made in various integral experiments on LR-0 [26].

The characterization of the neutron field in the graphite insertion is the main object of the given work. The field was characterized out by means of already validated on LR-0 dosimetric reaction rates of $^{197}\text{Au}(n,\gamma)$, $^{58}\text{Ni}(n,p)$, and $^{181}\text{Ta}(n,\gamma)$ reactions. In addition, other dosimetric reactions were validated in the obtained neutron field.

In general, the following subject was examined in the work. In the beginning, the general theory of integral experiments (1), problematics of cross-section validation (1.2), and examples of integral experiments on LR-0 (1.3) were explored. After that, on the practical example, the role of neutron filters was shown (1.4). Impacts of the Cd, Gd boron absorbers, and the graphite insertion on the neutron spectrum were demonstrated. Alteration of reaction rates portion for different reactions were displayed.

The theoretical part is continued by studying the reaction rates evaluation methods on LR-0. The method of the determination experimental reaction rates was described. At the end of the section, the main uncertainties in integral experiments were identified (2.3.1).

The next chapter (3) is related to methods of the efficiency calibration of HPGe detector on LR-0. The detector radiography, dead layer thickness, and Monte Carlo model of the detector was described. It is relevant to note that the great feature of the LR-0 spectrometry laboratory is the well-verified MCNP model of the HPGe detector. It allows to calculate the detector efficiency for any form of an activation sample quite precisely (with the 1.8 % bias). So it is possible to improve the irradiation conditions of a sample to decrease the statistical uncertainty of the peak measurement.

In the experimental part (4), two comparable parallel experiments with activation samples were carried out. The holder with activation samples was placed in the center of the graphite insertion among fuel assemblies. The MCNP model of the graphite core was prepared using the reference core model. Evaluation of the well-validated reactions such as $^{197}\text{Au}(n,\gamma)$, $^{58}\text{Ni}(n,p)$, $^{181}\text{Ta}(n,\gamma)$ showed that MCNP model characterizes the neutron field of the graphite core well. Based on this fact, reaction rates of the other dosimetric reactions were validated. The reactions were $^{63}\text{Cu}(n,\gamma)$, $^{54}\text{Fe}(n,p)$, $^{58}\text{Fe}(n,\gamma)$, $^{23}\text{Na}(n,\gamma)$, $^{64}\text{Zn}(n,\gamma)$. In the final section (4.3.1), the reaction rates uncertainties were analyzed.

Chapter 1

Integral Experiments

Two measurement approaches – differential and integral – are most often used for experimental studying nuclear data in neutronics. Each of them has its specific requirements of using, which defines its advantages and disadvantages. Usually, these two methods are applied separately but sometimes could be combined. The fundamental difference between them is in the measurement approach to the studied quantities. In differential experiments, a quantity is determined directly for a single value of parameter of quantity function. In an integral case, it is measured as the integral of these values.

For differential measurements, the monoenergetic neutron field should be used. It can be achieved by accelerators or neutron generators (D+T, D+D reactions, proton interaction with T, Li, Be, etc. [3]), but the reactions do not necessarily give a pure monoenergetic neutron beam. Moreover, it requires complex equipment (e.g., for time-of-flight method), lots of detectors, well-configured electronics, and high experience in data analyzing. Combination of errors in these factors significantly increase uncertainties of the measured quantity that is a big disadvantage of the differential method.

Integral quantities can usually be measured much more accurately than differential nuclear data, so it is tempting to use such data to tune evaluations to improve integral performance. Integral data imply spectrum averaged cross-sections or cross-section ratios, reaction rates, kinetic parameters, leakage spectra, scattered-neutron yields, multiplication factor, etc. Uncertainties are much lower in integral experiments than in differential. In particular, continuous (non-monoenergetic) neutron field is used, just one detector is needed for the measurement, and the evaluation procedure is direct and well described. It is possible to classify integral experiments based on different factors. For example, they may be divided depending on the investigated parameter. Generally, integral data imply spectrum-averaged cross-sections (SACS) or cross-section ratios, kinetic parameters, leakage spectra, scattered-neutron yields, multiplication fac-

tor, etc. [28]. Integral experiments also can be considered as "clean" experiments, "mock-ups", and "benchmarks" [6].

"Clean" experiments are focused on one single quantity (for example, cross-sections) in a simple environment so that calculations are made easily and precisely enough. The results of such measurements are more general and applicable to a large class of reactor calculations. On the other hand, the results do not take into account the complexity of the real system, that is a disadvantage. [6]

"Mock-up" experiments simulate the actual system, in all its materials and geometrical complexity. Such experiments reproduce as accurately as possible the conditions of the system under consideration. Then a more direct answer is received because all the sources of errors are included in their results. From the other side, the obtained uncertainties cannot be assigned to a certain step of the calculation (for instance, to distinguish between uncertainties in the nuclear data and the calculational procedure). As a result, there is no way to apply conclusions and errors of mock-ups on other systems, which are quite different from a simulated design. The best mock-up of a reactor is the reactor itself, but measurements on operating power reactors are rather limited by accessibility and by the adverse environment. Moreover, the results and conclusions of measurements on energetic reactors are typically private. [6]

"Benchmark" experiments are frequent and widely applied. They are usually used to check nuclear data and/or calculations methods. Such measurements are very detailed documented, so discussion and evaluation of likely errors are possible. Benchmarks can be very simple and "clean"; they can describe a realistic, complex system (e.g., critical condition in an actual power reactor) that can be used in order to check the final design methods. [6]

An example of a popular integral experiment is the measurement of criticality (when multiplication factor $k_{eff} = 1$) that can be determined with very high accuracy (by 0.1 pcm). However, it does not mean that experiment is precise because total uncertainty is not based just on k_{eff} but on the uncertainty of the critical configuration. So taking into account the chemical, isotopic and geometrical parameters of the system (e.g., the critical position of control rod). These parameters are usually known less accurately than k_{eff} itself. Material buckling measurements by exponential or pulsed techniques in subcritical facilities have frequently been carried out in the past. It was shown that these approaches are always less accurate than a proper calculation. Another application is validations of reactions cross-sections (see 1.2). [6]

1.1 Criteria for Nuclear Data Validation

Acceptability of results of integral experiments for validation of nuclear data is defined by following formal criteria [28]:

- Sensitivity only to a measured reaction channel.
- Measurement does not introduce correlations between other nuclides or reaction channels.
- High precision and accuracy in the measurement process.

According to these criteria, integral measurements can be divided into 4 classes. Those that fulfill all the above criteria belong to the 1st class. It can be spectrum averaged cross-section (SACS) in the standard neutron field (^{252}Cf , ^{235}U); or measurement of Maxwellian averaged cross-sections (MACS) in Maxwellian fields. [28]

The 2nd class contains conditionally acceptable experiments. It is supposed that more reliable data are not available, and experiments are sensitive only to a single reaction type, and no more reliable data are available. Examples of such experiments are measurements of activated samples in reactors, resonance integrals or spectrum averaged cross sections in well-defined neutron fields. [28]

The 3rd class involves experiments that are conditionally acceptable when no more reliable data are available. Generally, they help to understand significant cross-correlations. Criticality benchmarks can be modeled accurately and contain a minimum number of materials (used for specific libraries). [28]

Finally, in the 4th class, experiments that are not applicable to the evaluation process are used for data validation. For example, reactivity coefficient measurements, experiments on neutronics parameters from a power reactor, or complex criticality benchmarks. [28]

1.2 Validation of Neutron cross-sections

Nuclear cross-section is an effective area that quantifies the probability of a certain interaction between an incident particle and a target [25]. In other words, the microscopic cross-section defines the measure of probability with a nuclear reaction will occur. It is denoted by σ , and its unit is a barn (b), which equals 10^{-28} m². The cross-section is a function of follows: the type of reaction, the target nucleus, its temperature, the incident neutron energy (i.e., speed or temperature), and its relative angle between the target and the incident neutron [12].

When differential values of cross-sections are determined, it is necessary to fit them to continuous energy. Differential cross-sections are determined by independent laboratories; their values and fitting methods can be various. There is an example in Figure 1.1 to show discrepancies in cross-section for different libraries. As can be seen, usually, the problematic interval is in resonance area (for neutron capture reactions) and high energy region. Thus, validation of

cross-sections (namely fit used) is necessary. Validation is defined as the assessment of the accuracy of a model by comparison with experimental data that is independent of that used to derive the model. In integral experiments, it is possible to get an integral value of cross-sections SACS (spectrum average cross-sections) for the corresponding energy range. Then SACS can indicate if the fit was done correctly by comparison theoretical and experimental values of SACS. So integral experiments deal with this validation problematics very well if properly described, and uncertainties are acceptable. That is why one of the essential requirements of integral experiments is that a validation process must always report on the uncertainty of the experimental measurement and the uncertainty in the model's prediction. [28]

Laboratories, industry, and universities by the cooperative effort produce nuclear data libraries. Libraries contain data about cross-sections of different reactions. The most recent libraries: ENDF/B-VIII.0 (USA, 2018), ENDF/B-VII.1 (USA, 2011), JEFF-3.3 (Europe, 2017), JENDL-4.0u+ (Japan, 2016), CENDL-3.1 (China, 2009), BROND-3.1 (Russia, 2016), ROSFOND (Russia, 2010) [11]. Computational codes use nuclear data libraries to make the neutron calculation. For example, to perform the calculation of nuclear reactor cores or to determine the experimental conditions in irradiation facilities [28]. Moreover, the calculation of radiation parameters of materials for reactors and its concepts (e.g., fuel, moderators, reflectors, coolants) are being studied much. For example, FLiBe [27], FLiNa [19], graphite [26], steel [38], etc. Quantities of reactor dosimetry are received based on measurements of dosimetric reactions. Data about dosimetric reactions are contained in the library named International Reactor Dosimetry and Fusion File (IRDFF). Cross-sections of these reactions here are described more precisely and have lower uncertainties than in other libraries. The IRDFF-2 library contains data for 119 reactions important to the dosimetry community [36]. It should be noted that, unlike libraries mentioned, IRDFF is not a transport library, i.e., it does not include data for elastic and inelastic neutron scattering reaction, etc. Obvious examples of dosimetry reactions are reactor dosimetry reactions such as: $^{58}\text{Fe}(n,\gamma)^{59}\text{Fe}$, $^{54}\text{Fe}(n,p)^{54}\text{Mn}$, $^{58}\text{Ni}(n,p)^{58}\text{Co}$, $^{55}\text{Mn}(n,2n)^{54}\text{Mn}$, $^{46}\text{Ti}(n,p)^{46}\text{Sc}$, etc [40]. These materials are being used as reactor fluence monitors, that is used to determine neutron damage of reactor internals and vessel. Lots of cross-sections in the nuclear data libraries have already been evaluated, but substantial part of them still have relatively high uncertainties (mainly, in the resonance energy region). Hence there is a need in their experimental validation.

Integral experiments for cross-sections validation are based on irradiating activation materials in a well-described energy neutron spectrum. It is followed by measurements of the activity of these materials and calculation of cross-section according to calculation methodology. The most crucial factor here is precisely studied energy neutron field and a consistent uncertainties handling. So there are reference neutron fields. The spontaneous fission neutron source of

^{252}Cf is the best-characterized neutron benchmark field, which is the first neutron field standard [23]. It generally shows excellent agreement between the measured and calculated spectrum-averaged cross-sections for most reactions. The secondary standard is ^{235}U . It implies that a well-described region of the neutron spectrum of a research reactor (that uses ^{235}U) can be employed as a reference field. The reactor neutron field is affected by core components such as neutron transport in fuel, neutron transport in a moderator, neutron transport in core structural components [28]. There is no burning up of fuel in zero-power research reactors. Then ^{239}Pu is almost not being created, and the spectrum of ^{235}U stays "clear" (e.g., LR-0 or VR-1 research reactors in the Czech Republic). According to this, the neutron field of one of special cores LR-0 was defined as the reference benchmark field. Reference benchmark fields of research reactors are not so well-described as standard fields but considered as reproducible and permanent, which makes it acceptable as a measurement reference by a community of users. The IAEA community acknowledged the reference LR-0 neutron field. The well-validated MCNP model of the reference core proved that its neutron spectrum is indistinguishable from standard ^{235}U fission spectrum above 6 MeV [16].

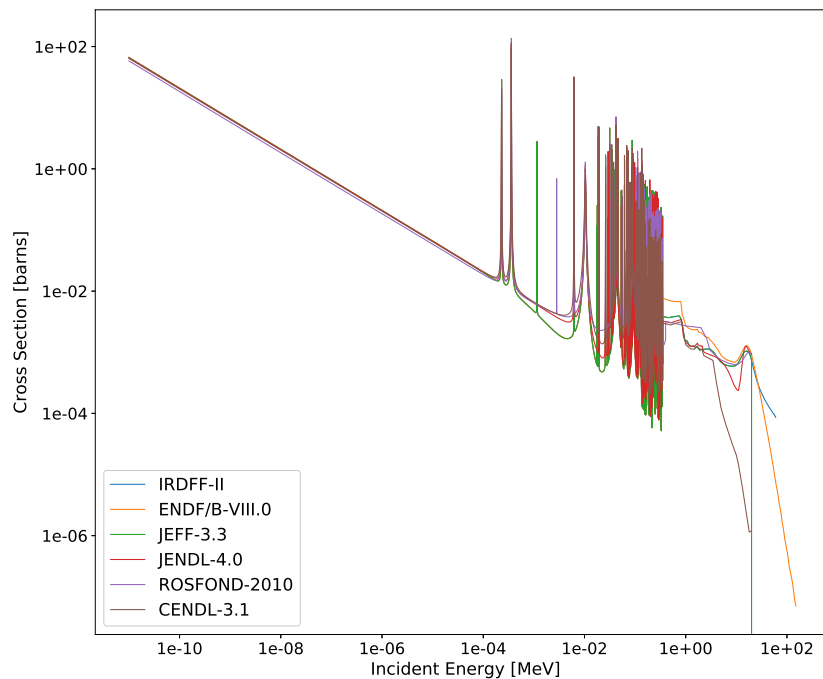


Figure 1.1: Cross-section for reactions $^{58}\text{Fe}(n,\gamma)^{59}\text{Fe}$ in different nuclear data libraries. [11]

1.3 Validation Integral Experiments in RC Řež

This thesis deals with an integral experiment on Research Centre Řež facilities. The results of cross-sections (SACS) validations by integral experiments are usually at a high level and well-appreciated by the IAEA and the IRDFF community. Therefore several such experiments on the LR-0 and 252-Cf are studied, and typical examples of integral measurements are given here.

The LR-0 is a zero power light water pool-type research reactor. It is constructed as an experimental reactor for measuring core characteristics for VVER 440/1000 type reactors. There are two types of criticality control: control-cluster (rods containing a boron carbide absorber B_4C), the moderator H_2O level, and the boric acid H_3BO_3 concentration. An AmBe emission neutron source is used to start the reactor. The reactor is suitable for various VVER-type configurations of the core, fuel enrichment (from 1.6 to 4.4 % ^{235}U), concentrations of H_3BO_3 in the moderator, additional moderators, and reflectors, configurations of absorptive elements in the fuel assemblies. The great feature of the LR-0 is a modular design of the supporting structures for reactor internals that allows adapting the core geometry and fuel parameters to the conditions of a large variety of experiments. So the reactor is primarily used for studying core insertion properties (inserted reactivity, spectral changes), neutron transport experiments, and cross-sections in benchmarked neutron fields. The scheme of the LR-0 reactor is in Figure 1.2. The basic characteristics of LR-0 are given in Table 1.1. [30]

For correct measuring and validation by integral experiments, it is necessary to have a well-characterized neutron field in a reactor. For this purpose, a precise mathematical model of a reactor core was made using the Monte Carlo particle transport codes. In order to verify the model and to characterize the field, measurements of well-validated reactions are required to correspond to simulation. For LR-0: the special core designed in Figure 1.3 was verified with the model by measurements and calculations in the publications: neutron and gamma spectra in [15] and [16], the power profile in [20], reactivity characteristic in [17], reaction rates of different dosimetric reactions in [21]. So it was proved that the central cavity of the given configuration is an excellent tool for validation of dosimetric cross-sections. Many validations of spectrum averaged cross-sections were carried out. For instance, for reactions (n,γ) and $(n,2n)$ on isotopes of zirconium [18]; $^{55}Mn(n,2n)$ and $^{127}(n,2n)$ [2]; graphite [26]. In general, LR-0 is an excellent tool for the whole library qualification. However, it might be disputable for some selected materials cross-sections because of the integration of many materials in the constructions of the reactor [28].

A spectrum of open ^{252}Cf is recognized as a standard. So SACS measurements can be performed without the validation process. On ^{252}Cf in Research Center Řež, a large set of cross-

sections from IRDFF library were measured. Many of them were published in [31] and [33]. ^{252}Cf is suitable for testing characteristics of materials so that the neutron source is covered by different materials in the form of a sphere or cube. In Research Center Řež, Fe, Ni, H₂O, D₂O, Pb spheres, and cubes of graphite, steel, Cu are available [28]. Results of validation SACS in such measurement can be found in [32] (nickel sphere) or [26] (graphite cube). Spherical benchmarks are an excellent tool for XS validation. There are better results than in cubes, perhaps, due to angularities. Also, neutron sources AmBe or PuBe are available and can be applied as potential experimental tools, but not so often used. In the case of reactor LVR-15 in Research Center Řež, integral measurements can be carried out as well. However, there are higher uncertainties in a model of fuel. There is 1 m silicon filter in the experimental reactor channel that causes a certain shaping of the neutron spectrum. For instance, it can be used for measurement of neutron transport and validation of SACS for reactions in lead [14].

Table 1.1: Basic characteristics of LR-0. [30]

Diameter of reactor vessel	3.5 m
Height of reactor vessel	6.5 m
Fuel type	VVER-1000 (Temelín NPP)/VVER-440 (Dukovany NPP)
Maximum power	1 kW
Flux density of thermal neutrons	$10^{13} \text{ m}^{-2} \text{ s}^{-1}$
Controlling method	level of the moderator, boric acid
Operating pressure	atmospheric
Operating temperature	room

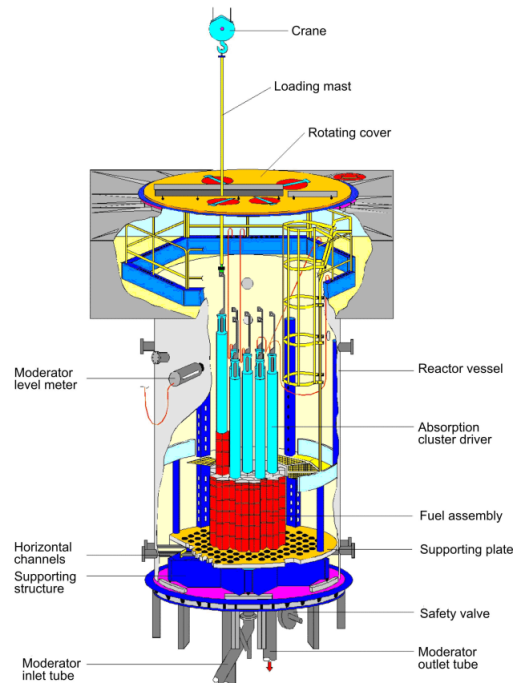


Figure 1.2: LR-0 scheme. [30]

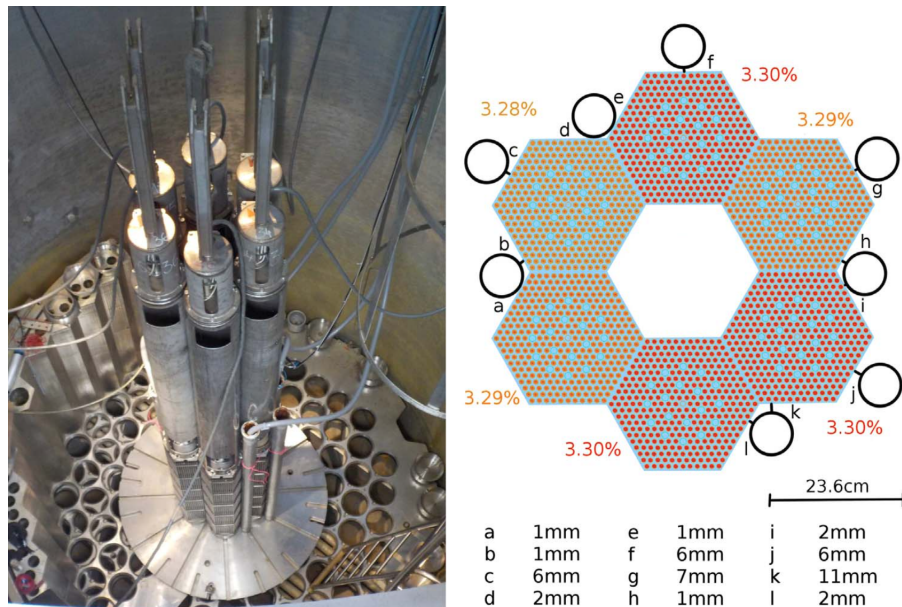


Figure 1.3: The view inside the reference core of LR-0 reactor (left) and its radial plot (right). [18]

1.4 Neutron Filters in Validation

Neutron filters can be applied in an integral experiment to test cross-sections in different energy regions. The neutron filter changes a spectrum by strong neutron absorption or/and neutron moderation in a particular energy range. Thus occurring reactions become more (or less) sensitive in a different energy region than in non-filtered spectra. That allows to determine the problematic region of the studied cross-section effectively. For radiation capture reactions, which are studied much as dosimetry reactions, filters suppressing thermal, and epithermal neutrons are applied. As a result, the radiation capture is initiated mainly by resonance neutrons and resonance integral can be derived. Comparing measured reaction rates for a bare sample and in the filter with calculated values, it is possible to evaluate if there are inaccuracies of cross-sections in the thermal or in the resonance region. The following materials are widely used as thermal neutrons filters: natural Cd, Gd, boron carbide B_4C , or boron nitride BN (with enriched ^{10}B) and In. Cadmium provides good neutron absorption below about 0.5 eV. Gadolinium is quite similar here, but it is a stronger absorber for larger energy. Boron has good attenuation for neutrons over a broader energy range from its $1/v$ absorption cross-section (from 1 to 10 eV depends on enrichment ^{10}B). The activation material is usually wrapped into the filter. [9]

As an example, the neutron spectra in filters in the cavity of the special graphite core of LR-0 (see 4.3) have been calculated and compared in Figure 1.4. Filters of Cd and Gd were represented in the MCNP calculation model as 1 mm spherical layer, B_4C as 4 mm for the natural compound of boron, and with 92 % enriched ^{10}B (according to the example in [36]). Moreover, the special graphite active zone of LR-0 can be considered as a neutron filter as well, because insertion moderates the spectrum of benchmark core greatly (see Figure 4.6). The result of using filters, experimental conditions for selected reactions improves, and it is possible to reproduce or disprove validation in the energy range of unfiltered neutrons. To show a specific example of using the graphite insertion and a neutron filter, the graphs are given in following Figures 1.6-1.9. The reaction rate share is shown to indicate to what extent different neutron spectra affect reaction rate. Absolute values of reaction rates in different spectra are different. Reaction rate fraction $q(E)$ is derived from calculated fluence φ , cross-section σ , and considering ∞ -energy as 20 MeV, as follows:

$$q(E) = \frac{\int_0^E \varphi(E)\sigma(E)dE}{\int_0^\infty \varphi(E)\sigma(E)dE}, \quad (1.1)$$

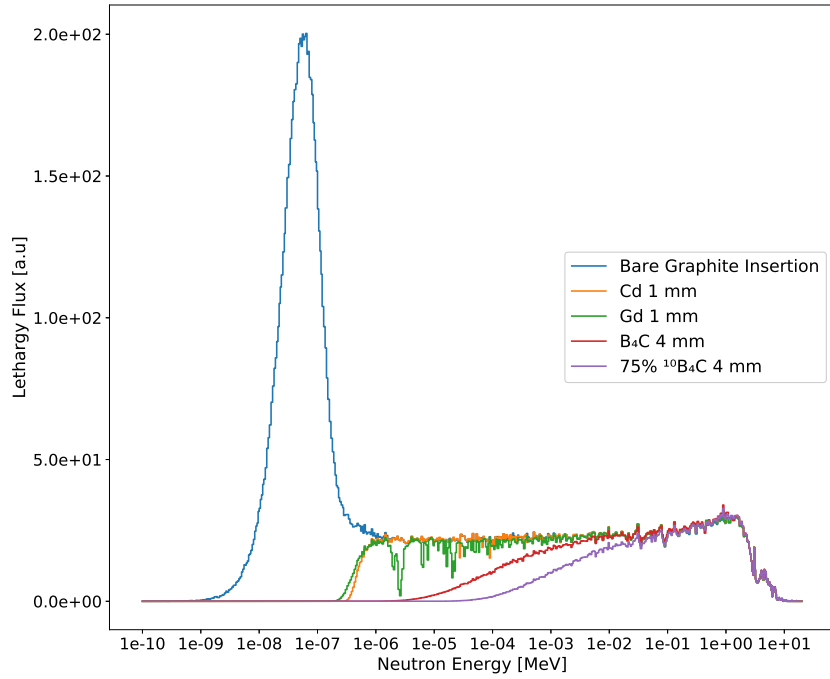


Figure 1.4: Unfiltered and filtered neutron fields in the special graphite core of LR-0 reactor.

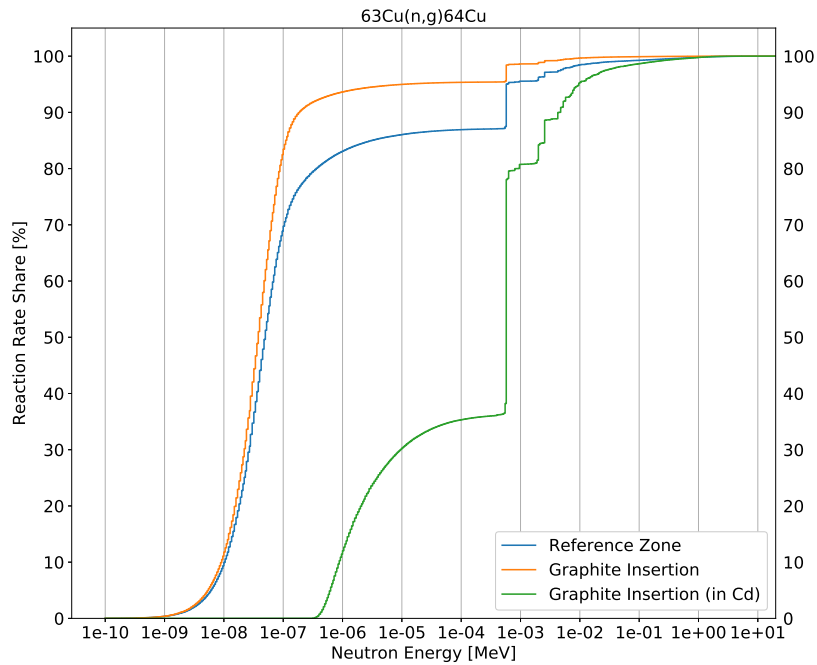


Figure 1.5: Reaction rate share for $^{63}\text{Cu}(n,\gamma)$ in different neutron spectra.

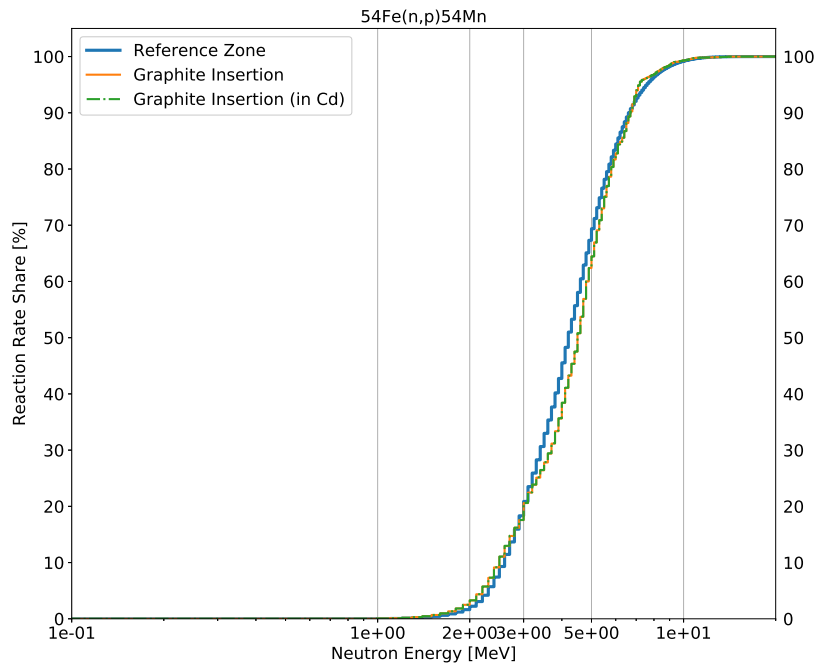


Figure 1.6: Reaction rate share for $^{54}\text{Fe}(n,p)$ in different neutron spectra.

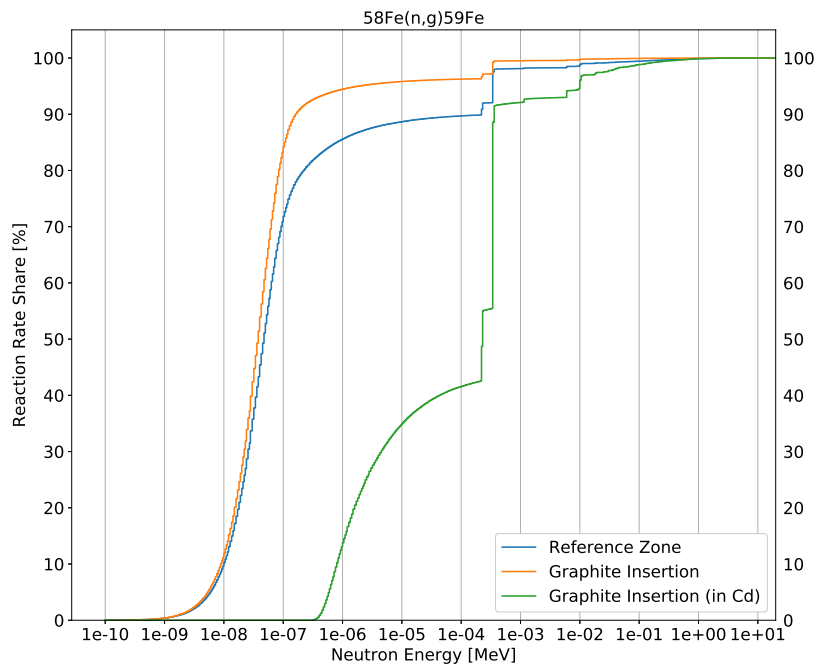


Figure 1.7: Reaction rate share for $^{58}\text{Fe}(n,\gamma)$ in different neutron spectra.

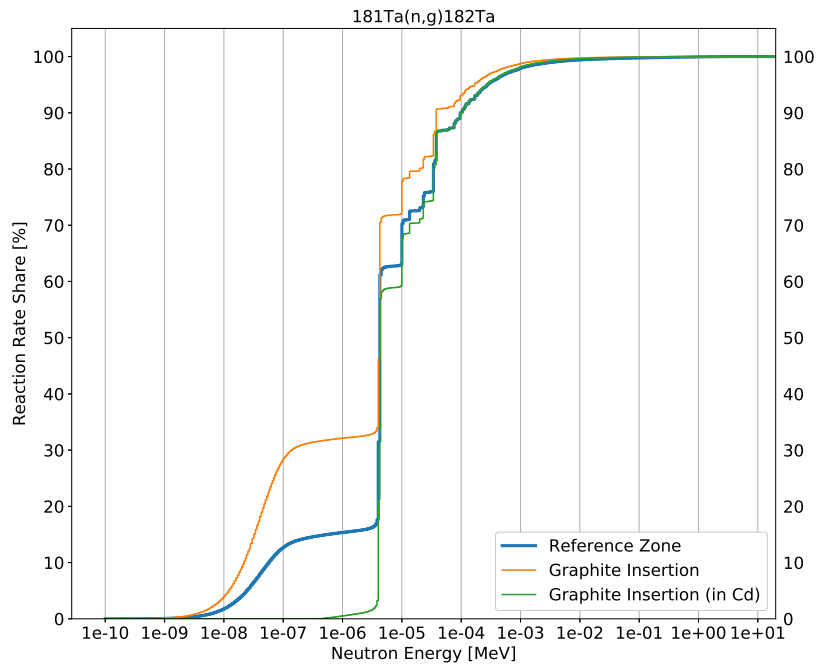


Figure 1.8: Reaction rate share for $^{181}\text{Ta}(n,\gamma)$ in different neutron spectra.

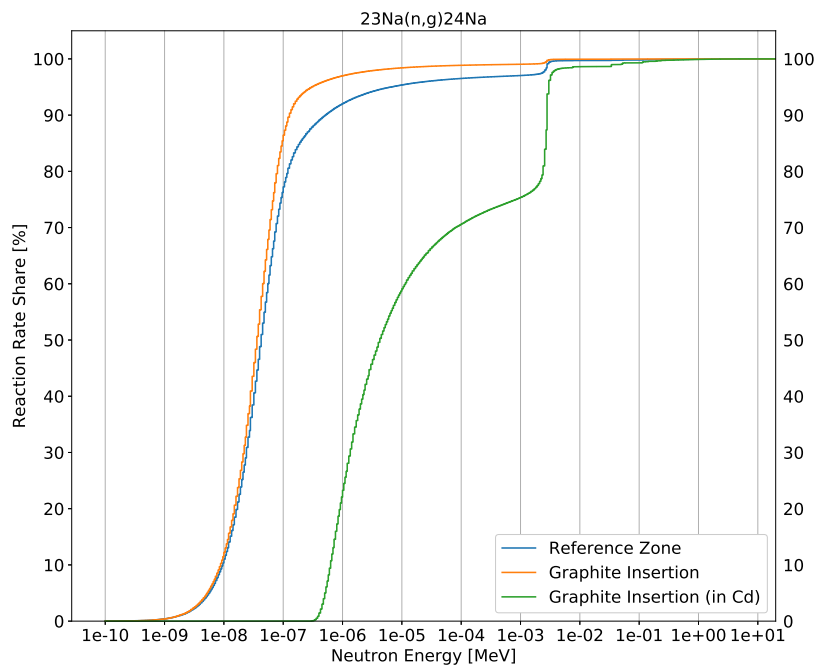


Figure 1.9: Reaction rate share for $^{23}\text{Na}(n,\gamma)$ in different neutron spectra.

Chapter 2

Evaluation of Reaction Rates on LR-0

The well-characterized neutron spectrum in the reactor is necessary for cross-sections measurement and validation. One of the essential steps in the characterization process of the spectrum is the determination of experimental reaction rates of well-validated neutron reactions.

In general, evaluation is a calculation procedure that is supposed to convert input quantity to comparable with significant physical quantity. So, in the case of neutron reaction rates, the input is the gamma activity of irradiated activation material in the reactor represented as a count rate measured by the detector. The output is reaction rate, whose values are compared with values calculated by model simulation. In this chapter, based on experience in similar experiments made in Research Centre Řež on LR-0 and Cf-252, the method of evaluation of reaction rates is described.

2.1 Activation experiments

Activation materials are placed in a reactor and irradiated with a neutron field. As a result of neutron reactions, artificially radioactive materials are created. The reaction rate (RR) is defined as the rate of radionuclide formation. In general, RR (denoted by q) can be determined as the multiplication of three parameters:

$$q = N_t \sigma I, \quad (2.1)$$

where N_t is the current number of target nuclei, σ is reaction cross-section, and the neutron flow density I hitting target activation material. If the product of the reaction is radioactive, its nuclei are decaying exponentially. During irradiation, the following equation should be applied:

$$\frac{dN}{dt} = -\lambda N + q, \quad (2.2)$$

where N is the number of radioactive nuclei, and $\lambda = \frac{\ln 2}{T_{1/2}}$ is the exponential decay constant. Then during irradiation N at the end of irradiation time t_{irr} follows the equation:

$$N(t_{irr}) = \frac{q}{\lambda}(1 - e^{-\lambda t_{irr}}) \quad (2.3)$$

In Figure 2.1, there is an illustration of dependence for the equation above. There is the maximum for this function, which can be obtained if $t_{irr} \rightarrow \infty$, then $N_{\infty} = \frac{q}{\lambda}$. The maximum is the saturated amount of radioactive nuclei and can be actually reached during ten half-lives $T_{1/2}$. Activity A is directly proportional to the activated amount $N - A = \lambda N(t)$. That means that the reaction rate is equal to saturated activity. However, it is not always possible to reach for long-term radioisotopes. Statistics of measurement are determined by the activity of irradiated material. To have better statistics, it is important to get as high activity as possible (in this case, saturated activity). So, activity depends on irradiation time, neutron flow density (reactor power or activity of neutron source), measurement conditions (detector efficiency for the selected geometry), and reaction cross-section and gamma branching ratio in the given decay. Then based on knowledge on these parameters, the needed irradiation time can be estimated so that to get eligible statistic uncertainty of measurement.

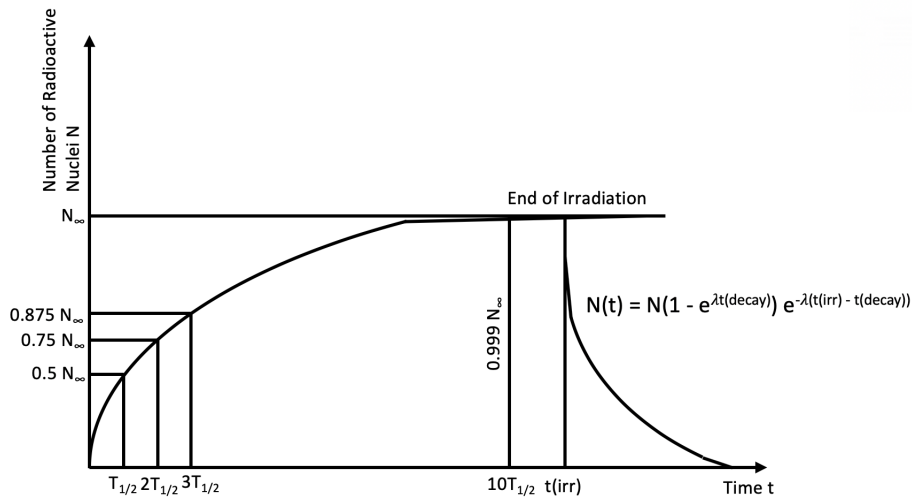


Figure 2.1: Production of radioisotopes on the time of irradiation. [1]

2.2 Experimental Reaction Rate

After activations, nuclei of radioactive isotope emits gamma photons with characteristic energy according to the occurred reaction and decay mode. Usually, to measure a spectrum of photons, gamma spectrometry by the HPGe (High Purity Germanium) detector is used. The

measured spectrum is represented as values of count rates for single energy channels. So emitted gamma rays from activated nucleus form visible peaks in the spectrum. The obtained gamma spectrum by the HPGe is analyzed Genie 2000 program (Canberra) [24]. The quantity called *Net Peak Area* (NPA) is calculated by Genie for each required peak in the spectrum. NPA is defined as the sum of count rates for all channels belonging to the peak subtracted by the background. The background radiation was measured without the sample when the detector was calibrated. Thus NPA directly presents the amount of activated nuclei N . Then the reaction rate q (the number of reaction per second in 1 cm³ of activation material) of activation at reactor power level \bar{P} is determined by the following equation [21]:

$$q(\bar{P}) = \left(\frac{A(\bar{P})}{A_{Sat}(\bar{P})} \right)^{-1} \times NPA(T_M) \times \frac{\lambda}{\varepsilon \times \eta \times N} \times \frac{t_{real}/t_{live}}{(1 - e^{-\lambda T_M})} \times \frac{1}{e^{-\lambda \Delta T}} \times k_{CSCF}, \quad (2.4)$$

where:

$\frac{A(\bar{P})}{A_{Sat}(\bar{P})}$ represents a relative portion of saturated activity induced during the irradiation; (2.2.1)

T_M is the time of measurement by HPGe detector;

$NPA(T_M)$ is the Net Peak Area (the measured number of counts for the given peak);

λ is the exponential decay constant ($\lambda = \frac{\ln 2}{T_{1/2}}$);

ε is the gamma branching ratio for the given gamma line;

η is the full-peak-energy efficiency of the HPGe detector (3);

N is the number of target isotope nuclei ($N = \rho \frac{N_A}{M}$);

t_{real} is the real time of the counting system of the HPGe (equals T_M); (2.2.2)

t_{live} is the live time of the counting system of the HPGe ($< t_{real}$); (2.2.2)

ΔT is the time between the end of irradiation and the start of HPGe measurement;

k_{CSCF} is coincidence summing correction effect factor; (2.2.3)

2.2.1 Relative Portion of Saturated Activity

In the equation 2.4, $\frac{A(\bar{P})}{A_{Sat}(\bar{P})} = \sum_i P_{rel}^i \times (1 - e^{-\lambda T_{irr}^i}) \times e^{-\lambda T_{end}^i}$, where:

P_{rel}^i is the relative power in the i-th interval of the irradiation period $P_{rel}^i = \frac{P^i}{\bar{P}}$;

T_{irr}^i is the irradiation time of the i-th interval of the irradiation period;

T_{end}^i is the time from the end of the i-th irradiation interval to end of irradiation period;

\bar{P} is the average power of the reactor.

This member of the equation 2.4 also provides correction for non-constant irradiation. Correction takes into account time to reach the power level \bar{P} and shutdown time before activated

material will be taken out from the reactor. Also, for cases, when irradiation lasts for a longer time and the reactor should be shut down for the night.

On LR-0, reactor power is measured by two independent ex-core systems of detectors. One is used to measure neutron flow density in the reactor core and then determines the reactor power [30]. So values of the LR-0 power during irradiation are represented as a count rate on the detector for single time intervals. Another is installed as a diverse system and mainly controls safety conditions.

2.2.2 Dead Time Correction

Ratio t_{real}/t_{live} in equation 2.4 expresses the dead time (also called resolving time) correction factor of the HPGe detector. Parameter t_{real} is the real time of measurement, t_{live} is the time that the detector was able to register gamma rays. Dead time is defined as a time interval needed for signal processing for one detected gamma photon. Thus the more often gamma rays hit the detector, the greater the loss of counts rate because of dead time effect. As a result, the value of NPA should be corrected. Dead time is analyzed by the HPGe spectrometry system and derived in the Genie 2000 program. If the dead time for an activated material is high (more than 5-10%), it can harm the detector. Then the source is placed further from the detector, or the measurements can be postponed until its activity decreases. Mostly the dead time factor is very low, and the correction is negligible.

2.2.3 Coincidence Summing Effect Correction

Coefficient k_{CSCF} in equation 2.4 represents coincidence summing correction. The effect occurs if two (or more) different gamma-rays emitted in a cascade from an excited nucleus are registered simultaneously (i.e., within the resolving time) by the HPGe detector. The detector cannot distinguish between them and identifies two interactions as a single event, where the energy transfer of the event is the sum of the energy of two interactions. As a result, it affects the real values of measured counts rates, and NPA values should be corrected. [39]

Two types of coincidence summing for an analyzed energy peak can occur – summing-in and summing-out. The summing-in effect results in the sum of counts at the energy corresponding to the sum of two energies. It may be that there is no gamma ray corresponding to the sum of energies then the new peak may appear at this energy. Summing-out is expressed from the loss of counts for these two single peaks. The k_{CSCF} is usually defined as a rate with the ratio of measured reaction rate to reaction rate without coincidence summing effect. Then it is less than unity for the summing-in and greater for the summing-out case. [39]

From the side of the activated nucleus, the coincidence summing depends primarily on the complexity of the decay scheme and probabilities of gamma-rays simultaneous emission, while it does not depend on the activity of the source. From the side of the measurement, it is very individual and dependent on the type of the detector (its efficiency) and the geometry of the measurement. The effect becomes more important at short source-to-detector distances, i.e., it strongly depends on the solid angle sustained by the detector. [34]

Most of the samples used in the measurement on LR-0 are considered or approximated as pointed (e.g., EG3 container that is an area source). Thus coincidence summing corrections are usually calculated by the method presented in [34]. Using the decay data, numerical equations for correction calculation of the selected gamma energy peak are made. Given equations contains two variables – the full-energy-peak efficiency and total efficiency of HPGe detector. They are obtained using MCNP simulation. True values of total efficiency are received as the difference between calculated total efficiency and efficiency for the first energy bin. The last presents efficiency for gamma-rays, which were flown through the sensitive volume of the detector without interaction. [34]

In the case of extended sources used (as in the [2] or [13]), they are discretized into pointed sources. So MCNP simulations are made for each segment. Discretization depth is determined by series of calculations with different segments number. This method is more precise, but the time required for efficiencies calculation can be very high. Then the method is not always suitable, and approximation is used. [5]

Moreover, the coincidence summing correction can be determined experimentally. It is made by the comparison of two measured reaction rates. In the first case, the source is located as far from the detector as it is possible to consider that coincidence summing effect can be neglected, and the activity of the source is still enough to measure with nice statistics. In the second, it is measured near or on the cap of the detector. This method is not used on LR-0 measurements, primarily because of the low activity of irradiated sources. [10]

2.2.4 Reaction Rate Normalization

The reaction rate obtained by equation 2.4 indicates a number of reactions in the selected sample per second. Here, the reaction rate corresponds to the neutron emission rate of the core (or to the average reactor power level). On the calculation side, reaction rates are usually received from the criticality simulation using the MCNP code [8]. For example, the program SERPENT can be used for such calculation as well, but MCNP is considered as transport and criticality calculations reference and more popular for validation purposes. In MCNP, fluxes and reaction rates are normalized by one source neutron in the generation in a volume of the

sample. The only average time spent in the volume of interest is missing [41]. Thus this time can be selected as 1 second. Thus calculated reaction rate will represent a number of reactions per second for one neutron in the considered volume of the sample.

Thus it is necessary to normalize measured reaction rates to calculated values to compare experimental and simulation results. The scaling factor is used. Its physical meaning is the neutron emission rate of the reactor core. The correction should be determined for each separate activation experiment. The scaling factor is derived from reaction rates in selected activation foil detectors, so-called monitors. The main requirement for the material of such detectors is a well-characterized and validated neutron cross-section of the selected reaction for the corresponding neutron energy spectrum. In activation experiments on LR-0, mainly two kinds of monitors are applied: gold (1 % in Al) and nickel (100 % Ni). In gold, the spectrum is evaluated for the 411.8 keV peak of the reaction $^{197}\text{Au}(n,\gamma)^{198}\text{Au}$. In nickel, the 810.8 keV peak of the reaction $^{58}\text{Ni}(n,p)^{58}\text{Co}$ is examined. These isotopes are chosen because their cross-sections are validated well, and used materials are monoisotopic, which minimizes the coincidence summing effect. In general, more activation foils of one material in various locations of the activation area are used to decrease the uncertainty of the scaling factor. [13]

Then the scaling factor K is defined as a ratio of the measured to calculated value of reaction rate in i -th activation foil detector:

$$K_i = \frac{q^i(\bar{P})}{q^i(1nps)}, \quad (2.5)$$

where $q^i(\bar{P})$ is a reaction rate for the emission rate of the reactor core per second, $q^i(1nps)$ is a reaction rate for one source neutron per second.

For N number of activation foil detectors:

$$K_{average} = \frac{1}{N} \sum_{i=1}^N K_i \quad (2.6)$$

Thus the values of measured reaction rates given by the equation 2.4 become normalized for 1 source neutron as follows:

$$q_{measured} = \frac{q(\bar{P})}{K_{average}} \quad (2.7)$$

2.2.5 Self-shielding Correction

Resonance self-shielding effect is the effect when the neutron flux is depleted due to absorption and scattering in the interior of the activation sample. Flux on the edge of the sample

does not equal to the flux in its center (that is considered as an experimental reaction rate). So that analyzed reaction rate is reduced and should be corrected to get true value. The effect occurs because of strong resonances in the cross-sections of radiation capture and elastic scattering reactions. The effect increases if resonance cross-sections are comparable to or higher than thermal cross-section. Resonance peaks are found at epithermal energies. In other words, the correction has to be made in case of activation on irradiation facilities that have a significant fraction of the epithermal neutrons in their spectrum. Moreover, strong thermal absorbers and moderators may also decrease the thermal flux inside the sample. Then the correction of the thermal self-shielding effect has to be made as well. Then self-shielding effects correction should be applied in activation on LR-0. Self-shielding effects depend on the neutron energy spectrum, the dimensions, and materials of the activation sample. [37]

Two Monte Carlo simulations are made to calculate the self-shielding correction. The fixed source model is applied here using flux calculated in the defined source model (that makes criticality simulation). In other words, the beginning part of the neutron evolution, which covers a detailed description of neutron origin in the fuel, is neglected. The factor is in good agreement, and the calculation efficiency is much better than using the defined source model [21].

A sphere with activation sample in the center is modeled, functions *sil*, *sp1* are used to define a fixed neutron source. Moreover, it is necessary not to set parameter *dir*=1 to keep the isotropic field. The output is set as a card *f4* and its modification *fm4* with numbers of the material and reaction and normalization to a barn - 10^{-24} . In the first simulation, the activation sample is presented as a void considering an analyzed reaction. Then there are no impact on the self-shielding effects. Then a real case is simulated. The self-shielding factor is determined as a ratio between two calculated reaction rates (without to with the sample). Then experimental reaction rates are multiplied by the factor. Reaction rates of thresholds reactions such as $^{54}\text{Fe}(n, p)$ or $^{58}\text{Ni}(n, p)$ are not affected by the self-shielding effects.

2.3 Evaluation of Reaction Rates

After all the necessary procedures have been applied to experimental reaction rates obtained by equation 2.4, they are being compared with calculated values. Calculation reaction rates are calculated for different nuclear data libraries using MCNP. Nowadays, the following libraries are commonly used: ENDF/B-VIII.0, JEFF-3.3, JENDL-4, CENDL-3.1, BROND-3.1. Typically one of the ENDF/B libraries is selected for transport and criticality calculation. It means that fission yields data of ^{235}U , and cross-sections of reactor materials use only this library. Then cross-sections of activation samples materials are used from all the common libraries.

If the sample was activated in the filter, the reaction rate is calculated in the 640-groups energy structure (SAND-II type). Then values of reaction rates are multiplied by the attenuation factors for the given filter, which are represented in the same group structure. The structure of 640-groups is commonly used by the evaluators to represent neutron spectra and cross-sections. Such division is enough so that more detailed groups of cross-sections do not differ negligibly. The energy span is from 10^{-10} MeV to 20 MeV. There are 45 energy groups per energy decade below 1 MeV and groups wide of 100 keV above 1 MeV. [42]

When reaction rates are received for various libraries, results can be evaluated, comparing them with experimental data. It is typically carried out by the calculated-to-experimental (C/E) ratio metric according to: $(\frac{RR_{calculation}}{RR_{experiment}} - 1) \times 100\%$.

The conclusion about the evaluation of one reaction should always be made based on results for several samples and/or in separate measurements. Moreover, accordance of different reactions should be considered to indicate if there is a fault of experimental or calculation approach. However, uncertainties are very deciding in evaluation. Usually the total uncertainty of measurement of most dosimetry reactions does not exceed 7 %, and uncertainty of calculation is about 1-2 %. Based on that, it is supposed that deviations C/E more than 10-15 % can indicate an issue in a nuclear data library.

2.3.1 Uncertainties

Conclusions about the evaluation strongly depend on its uncertainty. The total uncertainty is presented by calculational and experimental uncertainty. Calculational uncertainty is represented by:

- The stochastic error of the value that is caused by Monte Carlo (MC) method. It decreases by increasing the number of neutron generations simulated. The typical value is below 1%.
- Uncertainty in the fission source in the MC criticality simulations. In the LR-0 model, the system is defined as critical ($k_{eff}=1$), but it is not met exactly, because isotope ^{234}U is missing in the fuel model. Its concentration is extremely low, so the impact on the criticality as well - approximately about 100 pcm more. Then the error is about 0.1%.
- Uncertainty of the reactor description in the model. It includes mainly: uncertainty of the control rod position, the fuel radial or axial position, moderator critical height level, the activation samples positions. The total error for the LR-0 model is approximately 1.5%.
- Nuclear data uncertainty. In evaluated nuclear data files and individual libraries, cross-sections are presented with errors.

The value of the measurement uncertainty is calculated by applying the usual rules of error propagation for multiplicative and additive terms to 2.4. There are the following uncertainties:

- Stochastic uncertainty in gamma spectroscopy measurement. It implies the value of the gross peak area, the Compton continuum area, the background area and the parameters in the energy, and peak shape calibrations. The error strongly depends on the sample activity and time of counting.
- Stochastic uncertainties in the radionuclide half-time value, the reactor power level and shut-down time; measurement uncertainties in the mass and sample dimension, and composition of the sample. All of them are supposed as negligible in comparison with the count rate uncertainties.
- HPGe efficiency uncertainty. Statistical (MC) error of the computed HPGe efficiency (< 0.1%).
- Efficiency curve error that is given by the bias between calculated and measured HPGe response. For the HPGe MC model used in the work, it is 1.8% for point sources and 1% for Marinelli beaker. There is also uncertainty in the geometry of the measurement (<0.5%)
- Uncertainty of coincidence summing correction is defined by efficiency uncertainty.
- Uncertainty of the scaling factor for power level normalization. This is made by bias between Au and Ni foils based scaling factors. Reaction rate uncertainty is not considered here because statistical errors are low, and usually, variety of foils is used. Then the final uncertainty is made by standard uncertainty between standard deviations for each material, plus standard uncertainties for each material. Typically the error is below 4% using Au and Ni foils.
- Uncertainty from the bias between evaluated peaks. If an isotope has two or more evaluated peaks. Then the error is defined by standard uncertainty between activities for these peaks, plus their own uncertainties.
- Self-shielding correction statistical error (< 0.1%) from the fixed source Monte Carlo model.

Chapter 3

Efficiency Calibration of the HPGe Detector on LR-0

HPGe is a High Purity Germanium semiconductor detector. HPGe detector is the most often used detector in gamma spectrometry tasks, providing the best precision of the spectrum measurement. The main advantage of HPGe type detectors is the highest energy resolution. The energy required to make an ion pair is about 100 times smaller than in NaI(Tl) crystals and about 1.25 times smaller than in silicon crystals. Moreover, the silicon semiconductor detector is limited in its thickness (only a few millimeters), while germanium can have a depleted, sensitive thickness of centimeters. That is why it is much more effective in full energy absorptions for gamma rays up to MeVs. On the other side, HPGe detector should be cooled to the liquid nitrogen temperature (77 K) to reduce the thermal leakage current, but only during operation, while lithium drifted germanium detector Ge(Li) should be cooled constantly, that makes HPGe the best solution in gamma spectrometry.

To get an accurate value of the measured reaction rate of the activated sample, it is necessary to know the efficiency of the HPGe detector. Detector efficiency is defined as the probability that a photon will interact with a sensitive volume of the detector and transfer its energy to the detector. Generally, absolute efficiency depends on the detection photon energy and geometry of the measurement. Detector efficiency decreases with higher photon energy. A geometry dependence is presented by a solid angle between the source and the detector. Increasing a solid angle efficiency grows, because more photons can get into the sensitive volume of the detector.

There are total and full energy peak efficiency. Total efficiency is a ratio of the total number of detected photons and total number of photons emitted by the source. If a photon transfers its whole energy to the detector, it makes the full energy peak efficiency (it has no contribution in

case of coincidence summing). Not all photons energy should be absorbed by the detector if the photon reacts with the sensitive volume of the detector. Photons leak from the detector volume because of the Compton effect or electron-positron annihilation. Both efficiencies are important in the determination of experimental reaction rate: full energy peak – to calculate the activity of the source (see 2.2), total – coincidence summing correction (see 2.2.3).

Efficiency function is determined by the efficiency calibration procedure that can be realized by the experimental approach or mathematically using the Monte Carlo model. Experimental determination of the full peak energy efficiency is carried out using standard point sources emitted gamma photons in a wide range of energy. The efficiency is calculated as a ratio of the known activity of the standard to the measured activity by the detector. Dependence is determined by fitting the values of all calculated efficiencies. The main requirement is that all the sources should have similar dimensions and measurement geometry. The total efficiency is derived as the difference between the total number of counts and the background. However, experimentally it can be made only for mono-energetic radionuclides because, for two and more peaks, it is a problem to effectively distinguish which pulses belong to single peaks. The experimental approach is easy to apply, but on the other side, results usually have high relative uncertainty (5-10 %), which is not acceptable for validation integral measurements. Another big disadvantage is the experimental calibration can not be applied for sources with unusual shapes if sources with different dimensions were used for efficiency calibration.

In validation integral experiments, activation samples can have any dimensions, and the accuracy of activity measurement is significant. To avoid the experimental calibration disadvantages, a Monte Carlo model of the HPGe detector should be performed. The detector internal parameters should be precisely characterized to perform a Monte Carlo model.

3.1 Characterization of the HPGe Detector on LR-0

A closed-ended coaxial p-type HPGe (Ortec GEM35) detector is used for integral measurements in the LR-0 laboratory. A general scheme of the detector is given in Figure 3.1.

Accurate placements of all the involved parts of the detector play a role in the detection efficiency. Despite the fact the manufacturer of the HPGe detector provides all the needed internal parameters of the detector, they may be different for each detector of the same type. It is worth noting that, first of all, the model is prepared according to the datasheet from the manufacturer. Then the simulation and measurement for standard sources are compared. Sometimes such a model does not pass the verification. Then the detector parameters should be measured by users again. The detector characterization used on LR-0 was carried out according to the procedure provided by Czech Metrology Institute (CMI) [4].

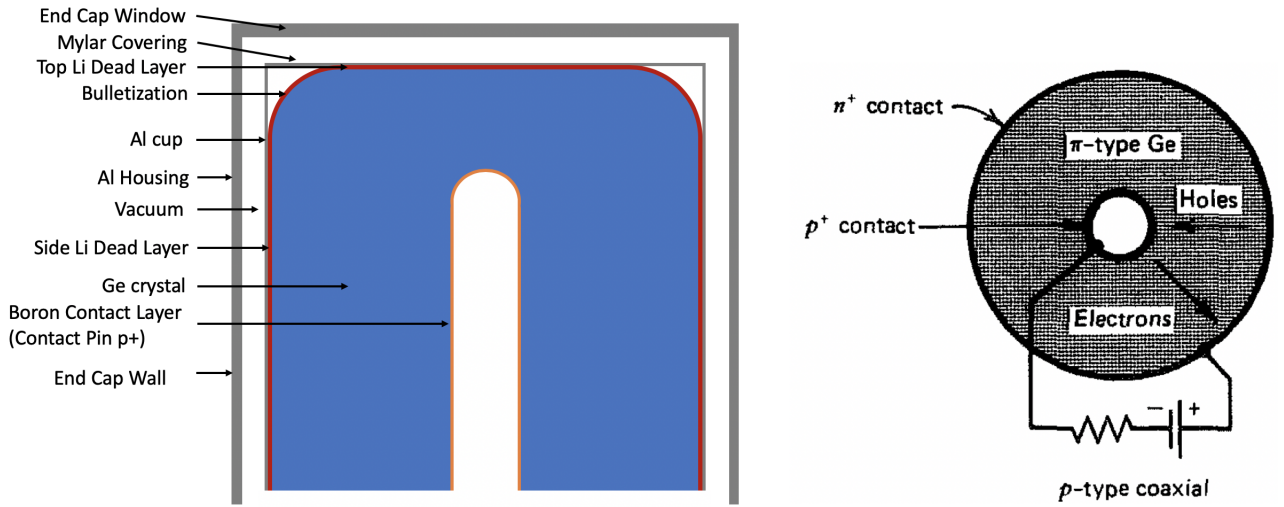


Figure 3.1: Scheme of the p-type HPGe detector: side view (left) [21], top view (right) [12].

3.1.1 Radiography

Radiography with gamma rays using ^{137}Cs source is applied to find out the detector dimensions. The picture of the radiogram is in Figure 3.2. There was determined the correction of the divergence of the ^{137}Cs source beam. The correction was presented as a ratio of an outer detector diameter on the radiogram and a real diameter. The divergence factor was 1.016. Dimensions used for the Monte Carlo model are given in Table 3.1. It was proven that the parameters in the detector datasheet are different from the data obtained from the radiogram. [1]

X-ray fluorescence is also used to measure the impurity concentration in the aluminum to get its accurate density [4].

Table 3.1: Detector parameters obtained from radiogram. [1]

Parameter	Measured value [cm]	Uncertainty [cm]
Crystal radius	3.003	0.010
Crystal length	5.525	0.020
Hole radius	0.482	0.011
Cap thickness (aluminum)	0.143	0.013
Pin radius	0.331	0.024
Pin contact length	0.369	0.026
Gap thickness	0.480	0.018



Figure 3.2: Picture of the HPGe detector radiogram (p-type Ortec GEM 35). [1]

3.1.2 Dead Layer Thickness

As a result of preparing a Ge crystal (as a p-type detector), the lithium dead layer is created on the outer side of the surface of the crystal. In a dead layer, the interactions between gamma photons and the crystal do not result in electrical signals. It leads to a loss of counts and a decrease of detection efficiency (mainly below 100 keV). The dead layer impact in detection efficiency is shown in Figure 3.3 [12].

The dead layer cannot be measured directly. For the boron implanted anode (n-type HPGe) it can be calculated with the data of the ion gun, but for the lithium diffused n-type cathode (mean-

ing p-type HPGe) it is impossible because there is not enough data on the diffusion constants of lithium in germanium crystals at room temperature and below. The lithium also diffuses further when the crystal is at room temperature what adds another uncertainty in efficiency. Therefore, the dead layer should be periodically remeasured. [7]

The Ge dead layer thickness is usually determined experimentally by measuring the attenuation of a collimated photon beam. The standard source of ^{241}Am is used because it emits gamma rays of 59.5 keV. It is enough low energy, so that influence of the dead layer is quite recognizable in measured counts. Collimators are used to direct a beam to the axial center crystal surface at angles of 30° , 45° , 60° , and 90° . It worth noting that there is a gap between the end cap and the crystal surface, thus the collimator must be moved so that the photon beams hit the same point on the crystal surface during all measurements. The gap and aluminum (cap) thickness are measured using the radiography. The dead layer thickness d_{dead} is derived from equation 3.1, which is based on the total number of gamma rays that got to the detector. Measurement should be made for many points on the surface of the detector to explore it for possible anomalies and to decrease uncertainty. Moreover, it is necessary to measure in front of the detector and on its side, because dead layers are typically different there. [4]

$$N_0 = N_\alpha / (e^{-\mu_{dead}d_{dead}\cos\alpha} e^{-\mu_{Al}d_{Al}\cos\alpha} e^{-\mu_{Mylar}d_{Mylar}\cos\alpha}) = N_\beta / (e^{-\mu_{dead}d_{dead}\cos\beta} e^{-\mu_{Al}d_{Al}\cos\beta} e^{-\mu_{Mylar}d_{Mylar}\cos\beta}), \quad (3.1)$$

following by:

$$d_{dead} = \frac{\ln(N_\alpha/N_\beta)}{\mu_{dead}\mu_{Al}d_{Al}\mu_{Mylar}d_{Mylar}(\sin\beta - \sin\alpha)^3} \quad (3.2)$$

where N_0 is the total number of emitted gamma rays got to the detector, $N_{\alpha,\beta}$ are a measured NPA for 59.5 keV peak for α, β angles of a beam, meaning numbers of gamma rays with this energy reached the sensitive layer of the detector; α, β are angles (in degrees) between the beam and the front surface of the detector; $\mu_{dead}, \mu_{Al}, \mu_{Mylar}$ and $d_{dead}, d_{Al}, d_{Mylar}$ are linear attenuation coefficients and thickness of a dead layer, an Al cap and a Mylar (polyester film covering the crystal). These thicknesses are derived from the radiogram as well.

For the HPGe detector in the LR-0 laboratory, two angles were used -45° and 90° . However, the uncertainty of the thickness was acceptable. The scheme of used beam collimator is in Figure 3.4. The measurements were performed at 33 points on the end-cap of the detector and at 12 points on the side of the detector (see Figure 3.5). Front dead layer thicknesses are shown in the 3D plot in Figure 3.6. Finally, the average of the front dead layer was 0.158 ± 0.003 cm, on the side was 0.121 ± 0.003 cm. These values were used in the Monte Carlo detector model.

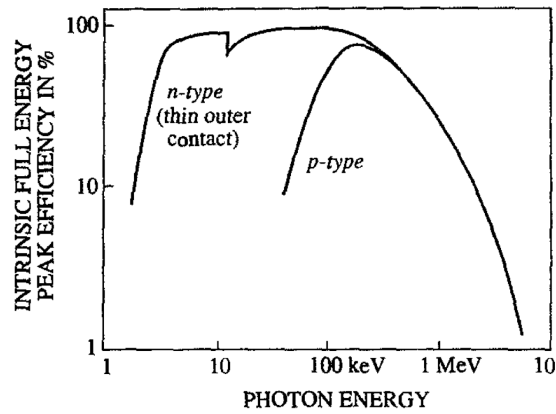


Figure 3.3: General character of inner peak efficiency for n- and p-type HPGe detectors. Efficiency is decreased by the dead layer at low energy region (n-type has thinner dead layer). [12]

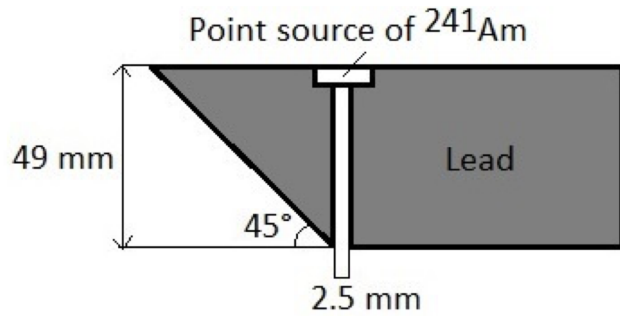


Figure 3.4: The photo (left) and the scheme (right) of the lead collimator for the dead layer thickness measurement. [1]

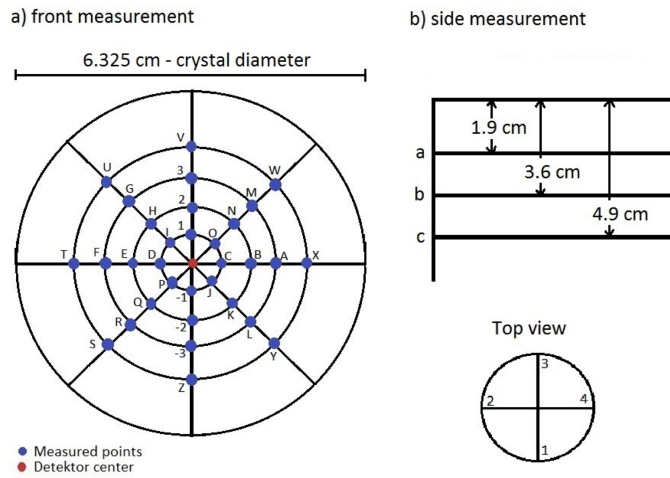


Figure 3.5: The dead layer measurement scheme (all distances between measured points on black lines are 6 mm). [1]

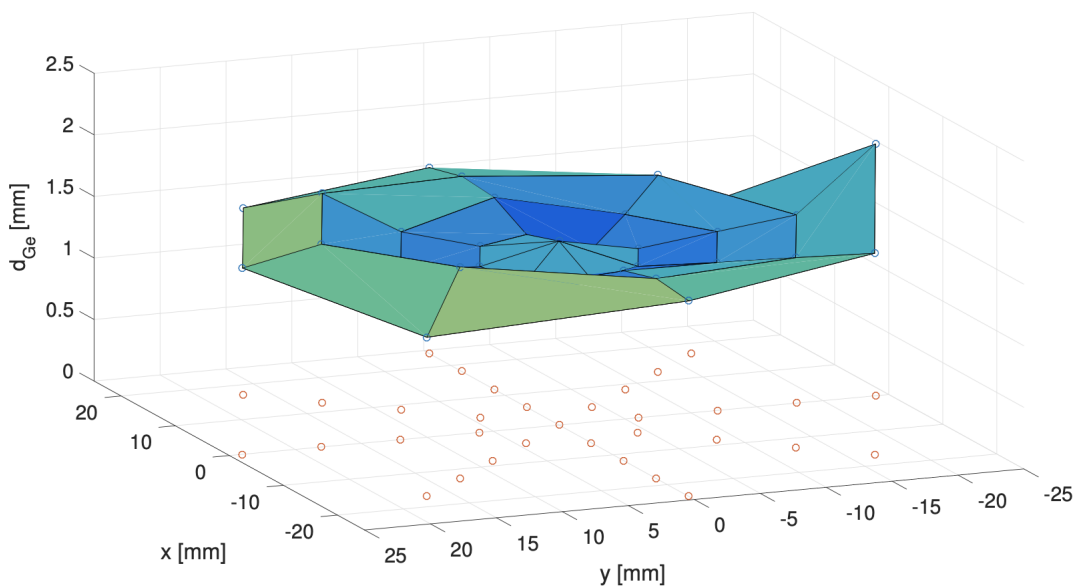


Figure 3.6: 3D graph of front dead layer thicknesses. [1]

3.2 Monte Carlo Model of the HPGe Detector on LR-0

Mentioned parameters are directly used to perform a precise Monte Carlo model of the detector. Monte Carlo simulation uses a pseudorandom number generator that makes it possible to accurately perform probabilistic events such as particle transport and interactions. The generated random numbers are assigned to the parameters of elementary particles. Then detector

efficiencies (total and full energy peak) can be calculated for any measurement geometry and gamma energy in the verified range. Monte Carlo simulations are usually made in the MCNP code [8].

Usually, the process of making a model has an iterative character. Experimental calibration is applied to verify the model. Changing internal parameters of the detector (within their uncertainty bounds, for example) is made to get as low as possible discrepancies between experimental and calculation values. The detector model is verified by comparing the calculated and measured full energy peak efficiencies for standard sources, which are usually used in the experimental calibration. For large-volume samples, typically of water solutions or soil, Marinelli beaker is used, and calibration is made for this geometry [12].

The exported image of the MCNP model of the p-type HPGe (Ortec GEM 35) detector used in the LR-0 laboratory is shown in Figure 3.7. For the given model, the discrepancy between calculation and experiment is about 1.8 % for the point source (e.g., EG3 container), which is also used for all other foils geometries (Fe block, NaF tablet). It is 1 % in Marinelli beaker geometry. Besides that, Monte Carlo efficiency has a statistical error that decreases by increasing the number of simulated neutron generations. For the model, 2×10^6 histories are enough to get the acceptable statistical error – less 0.1 %.

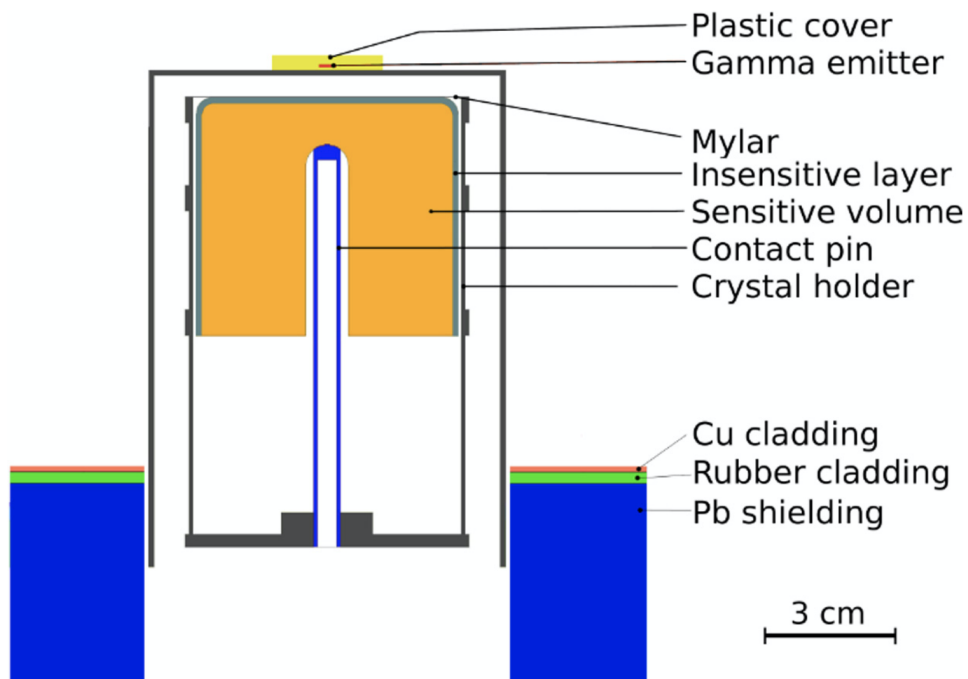


Figure 3.7: MCNP model of the HPGe detector with activated material in EG3 capsule. [21]

Chapter 4

Experimental Part

4.1 Description of Experiment

For the experimental part of this work, the graphite active of the LR-0 reactor was specifically assembled to make an integral experiment. Description of the LR-0 reactor and its experimental equipment was described in section 1.3.

The scheme of the core and fuel cartogram is given in Figure 4.3. Seven graphite blocks (shown red) were inserted between 12 fuel assemblies (shortened VVER-1000) with enrichment of 3.59 % and 3.6 %. Numbers of regular type of fuel assemblies are: 601, 607, 608, 610, 618, 619; Standard: 602, 604, 613, 614, 616, 617. Each graphite block is inserted into the own Al channel and consists of 6 trapezoid smaller blocks (see Figure). The density of the graphite is 1.72 g/cm^3 , with a purity of 0.2 ppm boron equivalent. The insertions were transported by a crane. As follows, fuel assemblies were installed. The central cavities in graphite blocks are filled by air.

The role of using the graphite insertion is the following: graphite is a strong neutron moderator, and its cross-section is well studied. Good moderation is provided by its low atomic weight (^{12}C), low neutron absorption cross-section, and high neutron scattering cross-section. Graphite nuclear properties are characterized well, because of wide experience in energetic nuclear reactors (Magnox, RBMK, etc.) and current high interest in generation IV reactors designs (HTGR - High temperature Graphite Reactor). For example, Czech small modular reactor Energy Well [29]. Moreover, graphite cross-section was already validated at LR-0 [26]. Then it is reasonable to use graphite insertion as neutron filter to change reference neutron field (very similar to ^{235}U fission spectrum) to test cross-sections in another energy region.

The purpose of the experiment is to characterize a neutron field in the cavity and make validation of reaction rates (or cross-sections). The characterization is based on the acceptable

agreement of simulation and calculation of already validated reactions. The activation should be carried out in the cavity of the central graphite block to get as much as possible a homogeneous neutron field. Activation samples are attached to the holder in the defined holes, which are drilled in the four pins (central and 3 in the circle with a 120° step). Holes are placed equidistant in pins. The holder is placed in this cavity by a crane. The scheme and picture of the holder are shown in Figure 4.4. According to the validation approach, two similar experiments were made to support the correctness of the experiment and to test more reactions. The holder is made of aluminum to minimize the impact of its activation. Al is often used as a suitable construction material as a quite less-activation and transparent for neutrons material than steel, for example. Aluminum is monoisotopic, i.e., it has only a single stable isotope – ^{27}Al . The most occurred reaction is $(n,\gamma)^{28}\text{Al}$ with 0.2 b for thermal neutrons and the biggest 3.6 b resonances for 6 keV [11].

The measurement parameters of the activation materials used are listed in Table 4.2. Smaller activation samples (Au, Cu, Ta, Ni foils) are placed in the holes, bigger (Fe blocks and Na tablets) are fixed by tape on them. Radiation capture (n,γ) reaction on ^{197}Au and (n,p) on ^{58}Ni samples are used to determine the scaling factors for flux monitoring. Cu, Fe, Ta, Na, Zn samples are used for the evaluation of cross-sections by means of reaction rate measurement.

Au and Ni foils are manufactured with standard dimensions so that to decrease parasitic effects (mainly self-shielding 2.2.5). Other samples have bigger dimensions but were tested and considered as suitable for experiments in LR-0 conditions.

The critical height was 40.315 cm and 40.383 cm. To compare: for 1 graphite block between 6 assemblies, the critical height was approximately 60 cm [35], which means less moderated core. Each activation lasted approximately 8 hours. The power (or neutron fluence) was measured as a neutron count rate by EX-core measurement and saved to further calculation of the relative portion of saturated activity (see 2.2.1). The average power was 1.5 % lower in the first than in the second experiment. There is no distinguishable difference between power levels during activations. Then the power level only for the first experiment shown in Figure 4.1. The reference time (used for determination of the average power) was picked at the moment closely before the power decrease.

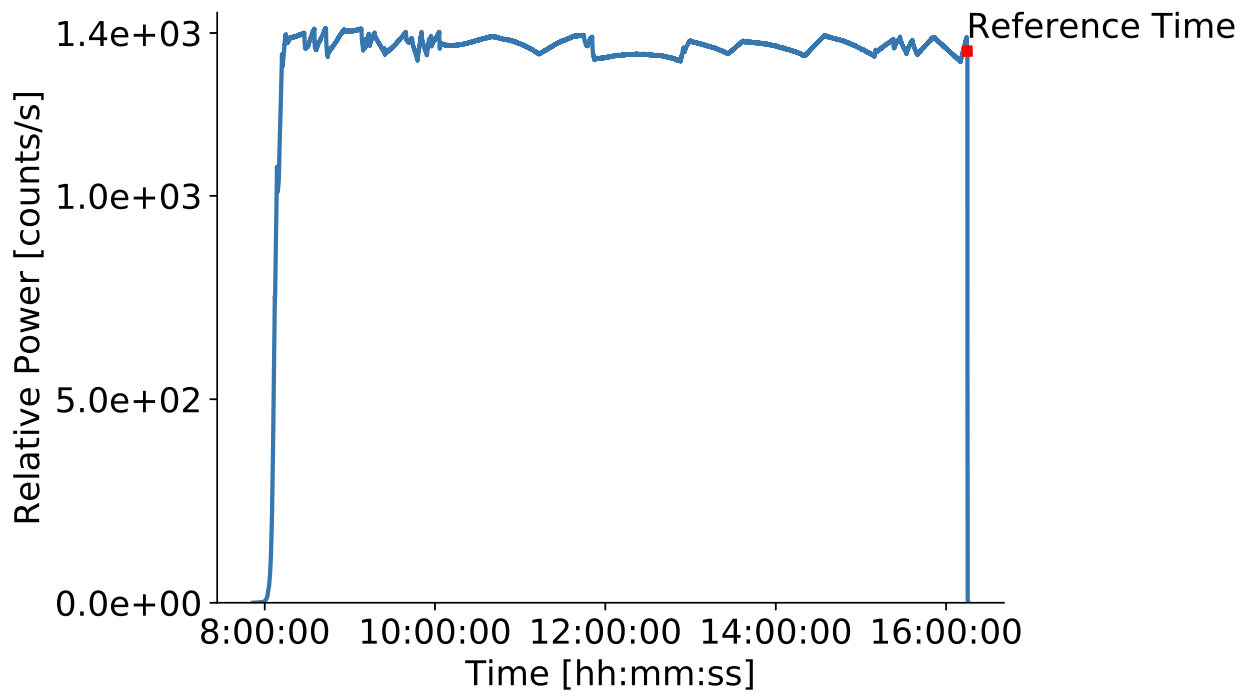


Figure 4.1: Relative power during activation.

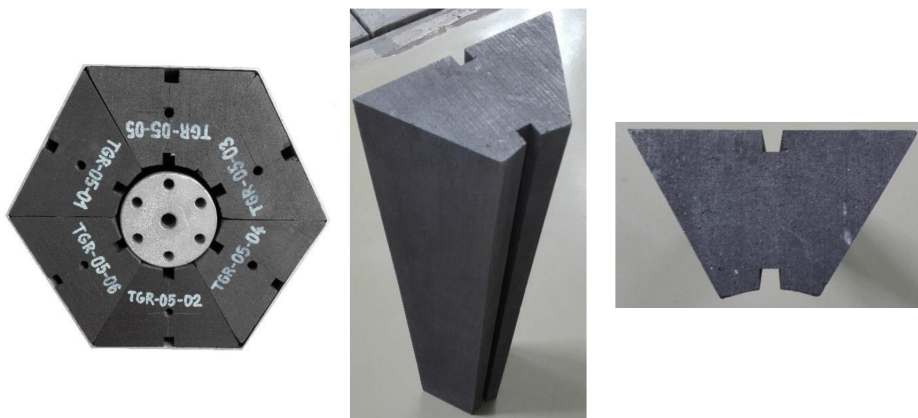


Figure 4.2: Construction of a graphite block. [35]

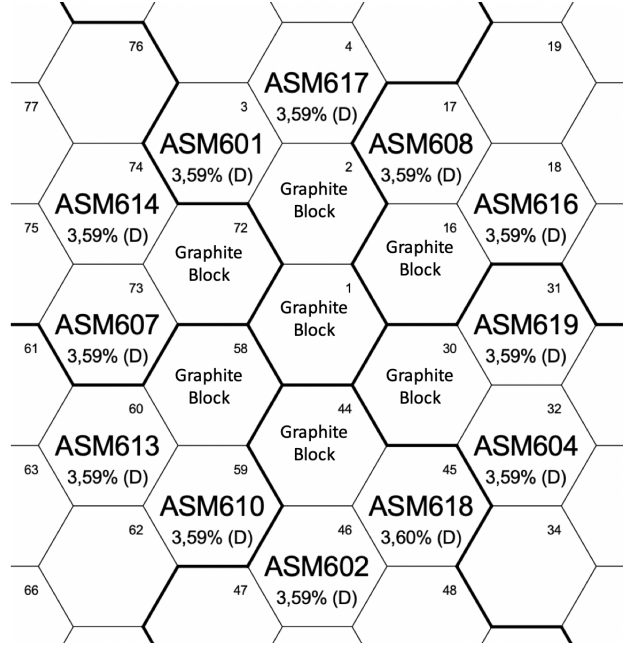
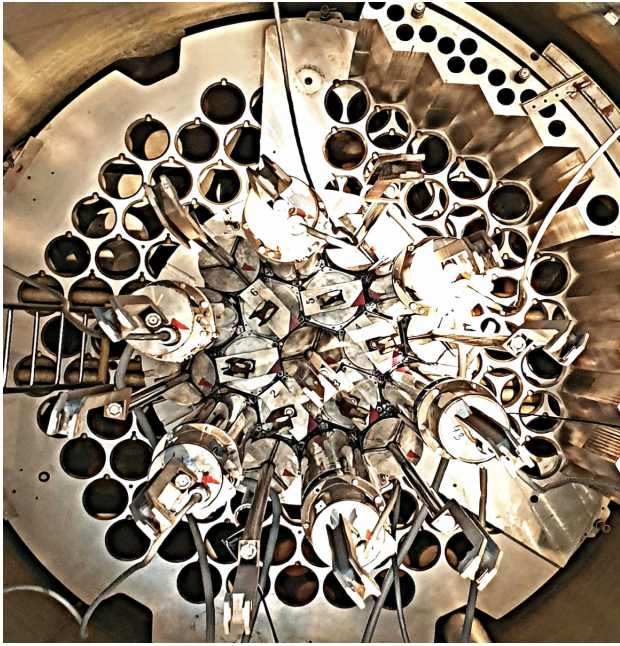


Figure 4.3: Overhead view at LR-0 reactor core with seven graphite blocks in the middle. The fuel loading cartogram to the right.

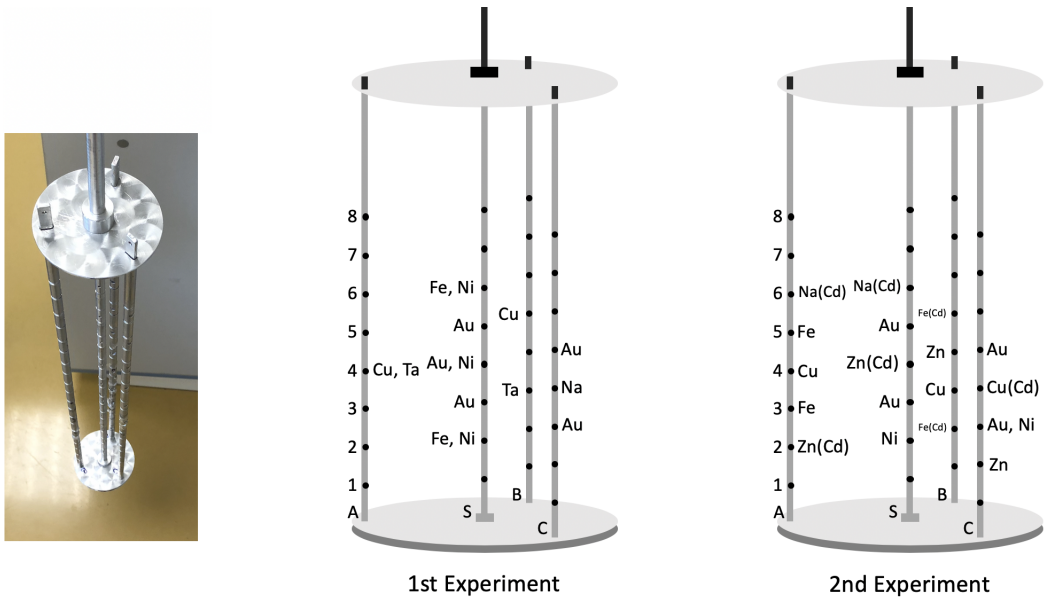


Figure 4.4: Picture and scheme of the holders with activation samples.

4.2 Monte Carlo Model of LR-0

4.2.1 Monte Carlo Computational Codes

Calculation codes are widely used in reactor physics and neutronics. Nuclear and particle interactions are simulated in codes. Simulation is based on computational and mathematical algorithms that are supported and validated by experimental data. Then a calculation code is a perfect tool that allows studying a wide range of neutronics and reactor parameters for any materials and geometry of the reactor without experimental measurements. For example, codes can be applied to modeling operating and emergency states, burning up history, or just receive neutron flux distribution in various locations of the reactor.

Nuclear decay, neutron, and other particle interactions are supposed as stochastic processes. Thus stochastic approach in calculation codes is the most suitable and accurate for particle transport simulations. Monte Carlo method is typically used there. Monte Carlo is a numerical method using the random number generator to calculate the average value of a stochastic quantity. The accuracy of the result directly depends on the amount of performed calculations. More attempts make the lower statistical error of the simulation. For example, neutron scattering parameters (such as direction, speed, and location of the next interaction) are randomly generated. Then making enough attempts of random generations, it is possible to obtain an accurate neutron path in the given material.

The worldwide codes using the Monte Carlo approach are MCNP [8] and Serpent [22]. Both have similar functions, but by evaluators community, MCNP is considered as a referenced code for cross-sections validation. Moreover, there are already validated models of the LR-0 in MCNP. Thus in the work, MCNP is used. The actual version of MCNP in 2020 is 6.2 [22].

4.2.2 Calculation MCNP Model of LR-0

The reactor core described in section 4.1 was modeled in the MCNP code to get data for core characterization and reaction rate validation. The given model was prepared using models of the reference active zone without (for example, [17] or [13]) and with graphite insertion [19]. The reference core consists of 6 fuel assemblies with a central cavity with a dimension of one fuel assembly.

Active zone (4.3) was modeled by true geometry corresponding to real dimensions and forms. The only simplification was applied here to supporting the fuel grid. Its form and dimensions were not changed, but it was homogenized with water, which is present in fuel assemblies. On the other side, it was shown it presents a negligible error ([19]). The main uncertainties of

the model are caused by hand manufacturing and assembly tolerances or uncertainty in the moderator level.

The model was adjusted by adding the holder used in the experiment. The horizontal and vertical view of the core model in MCNP is given in Figure 4.5. The holder dimensions were kept. However, the following simplification was applied: all the activation samples and holes in rods were represented as a void cylinder with the rod diameter (0.8 cm) and 0.8 cm height. The purpose of this replacement is to increase calculation effectivity, i. e. time of simulation for obtaining an acceptable statistical error. Sensitivity analysis and successful application for reference core [21] showed that this symmetric dimensions could be used.

The simulations were presented as criticality calculation with ^{235}U neutron source using MCNP function KCODE, which defines simulation conditions. It was set 4×10^4 source neutrons per one cycle, 2.5×10^5 active, and 50 inactive cycles. With these settings, one simulation lasted approximately 7 days using 16 processors. The error of the output reaction rates for the most reactions is less 1 %.

All material cross-sections and neutron emission spectrum were defined using ENDF/B-VIII.0 nuclear data library, while ENDF/B-VII.0 (and 1) is licensed as a reference for LR-0 analyses. Only the activation rates of the sample were calculated with the cross-sections from different libraries. Tallies f4 with e4 (including 640-group energy distribution) were used to get neutron fluence in locations of samples. Reaction rates for IRDFF-2 library were obtained by the scalar multiplication of neutron fluence and its cross-sections. Reaction rates for other libraries were determined directly from MCNP. In this case, fm cards were added to set analyzed isotopes and reactions.

It is necessary to note that multiplication factor k_{eff} from criticality simulation is not always exactly 1. Usually, it is tens or hundreds of pcm (percent mille - 10^{-5}) more than 1. For the given model – 117 pcm. This value corresponds to the estimation of the concentration of isotope ^{234}U in the fuel that is absent in the MCNP model. It is not sufficient correction, but it is correct to divide them by received k_{eff} to normalize calculated reaction rates. The effect of gamma transport is neglected in the model since it has been shown in [17] that it is negligible in terms of (γ, n) reaction contributions to the measured reaction rates [21].

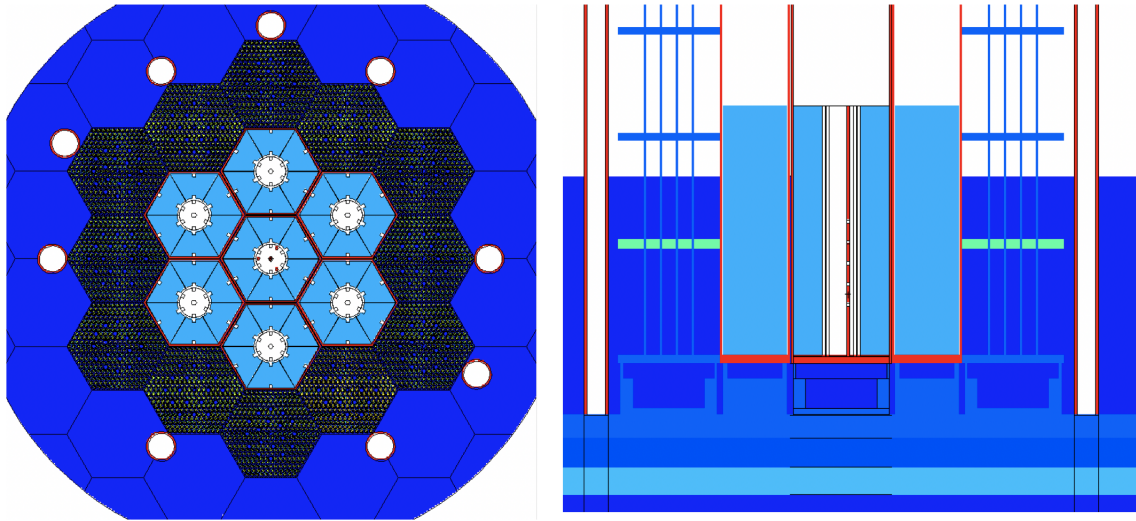


Figure 4.5: Special graphite core of LR-0 reactor with holder in the centre cavity in MCNP model.

4.3 Results and Uncertainties

Calculated neutron spectra in the central cavity of the core with 7 graphite blocks and of the reference core are shown in Figure 4.6. Neutron fluxes are given as lethargy flux, normalized in 1 eV to 20 MeV range for more convenient comparison. Spectra are presented for the position S2 of the holder (Figure 4.4). Also, the spectrum with Cd filter is shown. As can be seen, the peak around 2 MeV (emitted from ^{235}U fission) is strongly moved by graphite moderator to the thermal region.

The $^{197}\text{Au}(n,\gamma)$ and $^{58}\text{Ni}(n,p)$ reactions were used for the determination of the scaling factor, which illustrates the averaged neutron emission in the core. The parameters of scaling factors are introduced in Table 4.1. The averaged reaction rates are given: five and four Au foils, two and two Ni foils were used in the 1st and 2nd experiments, respectively. Scaling factors of single foils are in good agreement. The standard deviation of Au scaling factors is 2.36% in the 1st experiment, and 3.81 % in the 2nd. The standard deviation of Ni scaling factors is 1.50% in the 1st experiment, and 2.60% in the 2nd. The scaling factor in the 2nd experiment is higher than in the first a bit. That corresponds to the relation between averaged power levels derived from EX-core measurements. Using scaling factors, the other measured reaction rates were scaled to unit emission and compared to the calculation made in different nuclear data libraries. It was made for $^{63}\text{Cu}(n,\gamma)$, $^{54}\text{Fe}(n,p)$, $^{58}\text{Fe}(n,\gamma)$, $^{181}\text{Ta}(n,\gamma)$, $^{23}\text{Na}(n,\gamma)$, $^{64}\text{Zn}(n,\gamma)$ reactions.

The selected parameters of measurements of the activation samples are given in Table 4.2. HPGe efficiencies were calculated again using MCNP model despite the fact that they were

known from past experiments. Coincidence summing factors of approximated pointed sources were determined as well using equations in [34]. As evidenced, the higher energy corresponds to the lower efficiency. Comparing $^{58}\text{Fe}(n,\gamma)$ and $^{181}\text{Ta}(n,\gamma)$, efficiency for 1099.2 keV from Fe is lower than for 1121.3 keV from Ta. That is primarily due to gamma self-shielding effects in samples themselves. Fe block is 25 times thicker than Ta foil (0.0127 cm), and the density of Fe is 7 times higher than EG3 case of PMMA plastic, where Ta foil is placed. Moreover, there is a lower solid angle between Fe block and the detector than for Ta foil. The same reasons are valid for 1368.6 keV from NaF sample. In the case of NaF measurements, two more distant geometries were used due to higher activities. Then their efficiencies are much lower, while coincidence summing factor became higher (that means less effect) due to larger distance from the detector.

Self-shielding factors used are followed in Table 4.3. There are also factors for the LR-0 reference core. As seen, factors of Au, Na, Ta, Zn are lower for the graphite core. Resonances in their cross-sections have less impact because of less resonance neutrons portion in the graphite core spectrum. However, the self-shielding impact for these reactions increases by using Cd because of high thermal absorption. The self-shielding factor of Fe is higher for the graphite core. This reaction has narrower and less significant resonances, while its thermal cross-section is quite high in comparison with resonances. Then the self-shielding effect decreases in Cd filter.

Experimental reaction rates, which were corrected and normalized on one source neutron per second, are followed in Table 4.4. A comparison of experimental and calculated reaction rates of different reactions are presented for both experiments in Figures 4.7-4.12. Each plot contains the comparison for one material. Total uncertainties are indicated using dotted lines. All the reaction rates values and uncertainties are presented in the Appendix A. Uncertainties analysis is followed in the next subsection 4.3.1.

Reaction $^{63}\text{Cu}(n,\gamma)$ – Fig. 4.7. Only one sample (2nd experiment position A4) is in good agreement with all libraries; other samples have much larger discrepancies than uncertainties. As indicated, C/E-1 values are only positive, that means experimental reaction rates are under-valued by libraries.

Reaction $^{54}\text{Fe}(n,p)$ – Fig. 4.8. It can be assumed that results agree well, but only taking into account the fact that discrepancies are within uncertainties. The reaction threshold is 0.7 MeV, while there is a lower share of fast neutrons in the spectrum. As a result, uncertainties are very high (up to 18%) due to a low statistic of the peak measurement. Based on this, a correct evaluation can not be made. In the further experiments on LR-0, the reaction (in Cd as well) will be revalidated by improving the irradiation conditions.

Reaction $^{58}\text{Fe}(n,\gamma)$ – Fig. 4.9. As illustrated, most results for bare samples match to nu-

clear libraries results except ENDF/B-VII.1 and ROSFOND-2010. As evident, the data have been corrected in the newer ENDF/B-VIII.0, because discrepancies are much lower there. Concerning samples in Cd, the agreement is quite similar but it can be noticed that most libraries overestimate experiment. However, it is suitable to reduce statistical uncertainties of measurements to get a clearer picture.

Reaction $^{64}\text{Zn}(n,\gamma)$ – Fig. 4.10. The reaction is not dosimetric and not included in IRDFF libraries. All the represented libraries overpredict the experiment, both for a bare sample and in Cd.

Reaction $^{181}\text{Ta}(n,\gamma)$ – Fig. 4.11. As can be observed, there is a good agreement for most libraries within uncertainties. The outcomes reproduce agreements for Ta in [21], where the reference core was characterized. The achieved agreement supports the satisfactory characterization of the graphite core. As for the reference spectrum was shown, there is significant calculational overprediction of the experiment, up to 9.72 % in case of ENDF/B libraries.

Reaction $^{23}\text{Na}(n,\gamma)$ – Fig. 4.12. Experimental values meet calculational results for bare samples very well. The sample in Cd indicates a large discrepancy that is greatly exceeding the total uncertainty. Moreover, it should be pointed out that both bare samples are from different experiments. Based on this, it could be evaluated that cross-section of $^{23}\text{Na}(n,\gamma)$ reaction have some inaccuracies in the resonance region. As can be noticed, these inaccuracies do not reflect on results for bare samples much. It could be expected because there is a far larger portion of thermal neutrons than resonance neutrons in the spectrum of the graphite insertion.

Table 4.1: Parameters of scaling factors for two experiments.

Quantity	1st Experiment	2nd Experiment
$\langle q_{Au}^{exp} \rangle$ [s^{-1}]	4.145E-15	4.138E-15
$\langle q_{Au}^{calc} \rangle$ [s^{-1}]	8.282E-27	8.261E-27
K_{Au}	5.006E+11	5.009E+11
$\langle q_{Ni}^{exp} \rangle$ [s^{-1}]	2.276E-19	2.177E-19
$\langle q_{Ni}^{calc} \rangle$ [s^{-1}]	4.529E-31	4.323E-31
K_{Ni}	5.023E+11	5.036E+11
$K_{average}$	5.014E+11	5.023E+11
Total Uncertainty [%]	2.808	3.833

Table 4.2: Measurement parameters of the activation samples.

Reaction	Sample Type	Geometry	E_γ [keV]	η_{HPGe} [-]	k_{CSCF} [-]
$^{197}\text{Au}(n,\gamma)^{198}\text{Au}$	1% Au foil	EG3, on the cap	411.8	0.0829	0.998
$^{63}\text{Cu}(n,\gamma)^{64}\text{Cu}$	Cu foil	EG3, on the cap	511.0	0.0685	1.000
$^{58}\text{Ni}(n,p)^{58}\text{Co}$	Ni block	bare, on the cap	810.8	0.0460	0.933
$^{54}\text{Fe}(n,p)^{54}\text{Mn}$	Fe block	bare, on the cap	834.8	0.0416	1.000
$^{58}\text{Fe}(n,\gamma)^{59}\text{Fe}$	Fe block	bare, on the cap	1099.2	0.0337	0.988
			1291.6	0.0297	0.990
$^{181}\text{Ta}(n,\gamma)^{182}\text{Ta}$	Ta foil	EG3, on the cap	1121.3	0.0353	0.867
			1221.4	0.0329	0.940
$^{23}\text{Na}(n,\gamma)^{24}\text{Na}$	NaF tablet	bare, on the cap		0.0301	0.859
		5 cm	1368.6	0.0041	0.983
		10 cm		0.0016	0.993

Table 4.3: Self-shielding correction factors for two LR-0 cores.

Reaction	Form	Graphite Insertion [-]	Reference Core [-]
$^{197}\text{Au}(n,\gamma)^{198}\text{Au}$	bare	1.0187	1.0269
$^{63}\text{Cu}(n,\gamma)^{64}\text{Cu}$	bare	1.0261	-
	in Cd	1.2515	-
$^{58}\text{Fe}(n,\gamma)^{59}\text{Fe}$	bare	1.0520	1.0310
	in Cd	1.0136	-
$^{181}\text{Ta}(n,\gamma)^{182}\text{Ta}$	bare	1.9824	2.2892
	in Cd	-	2.8663
$^{23}\text{Na}(n,\gamma)^{24}\text{Na}$	bare	1.0058	1.0102
	in Cd	1.0529	1.0658

Table 4.4: Experimental reaction rates (normalized and corrected).

Reaction-position	q_{exp} [s^{-1}]	Reaction-position	q_{exp} [s^{-1}]	Reaction-position	q_{exp} [s^{-1}]
$^{63}\text{Cu}(n,\gamma)$ -A4-1	1.705E-28	$^{58}\text{Fe}(n,\gamma)$ -S2	4.987E-29	$^{64}\text{Zn}(n,\gamma)$ -S4 (Cd)	4.047E-30
$^{63}\text{Cu}(n,\gamma)$ -A4-2	1.791E-28	$^{58}\text{Fe}(n,\gamma)$ -S6	5.184E-29	$^{64}\text{Zn}(n,\gamma)$ -A2 (Cd)	3.408E-30
$^{63}\text{Cu}(n,\gamma)$ -B3	1.690E-28	$^{58}\text{Fe}(n,\gamma)$ -A3	5.201E-29	$^{181}\text{Ta}(n,\gamma)$ -A4	2.972E-27
$^{63}\text{Cu}(n,\gamma)$ -B5	1.667E-28	$^{58}\text{Fe}(n,\gamma)$ -A5	5.330E-29	$^{181}\text{Ta}(n,\gamma)$ -B3	2.706E-27
$^{63}\text{Cu}(n,\gamma)$ -C4 (Cd)	1.351E-29	$^{58}\text{Fe}(n,\gamma)$ -B2 (Cd)	3.031E-30	$^{23}\text{Na}(n,\gamma)$ -A6	1.888E-29
$^{54}\text{Fe}(n,p)$ -S2	2.920E-31	$^{58}\text{Fe}(n,\gamma)$ -B5 (Cd)	3.601E-30	$^{23}\text{Na}(n,\gamma)$ -C4	2.173E-29
$^{54}\text{Fe}(n,p)$ -S6	2.835E-31	$^{64}\text{Zn}(n,\gamma)$ -B4	3.104E-29	$^{23}\text{Na}(n,\gamma)$ -S6 (Cd)	9.049E-31
$^{54}\text{Fe}(n,p)$ -A5	3.371E-31	$^{64}\text{Zn}(n,\gamma)$ -C2	2.763E-29		

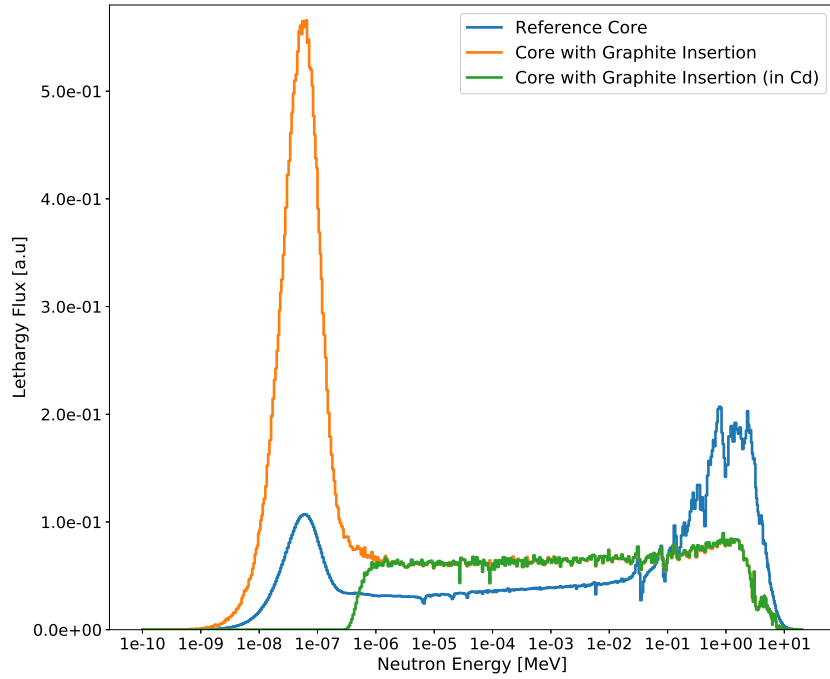


Figure 4.6: Calculated neutron spectra in two LR-0 cores.

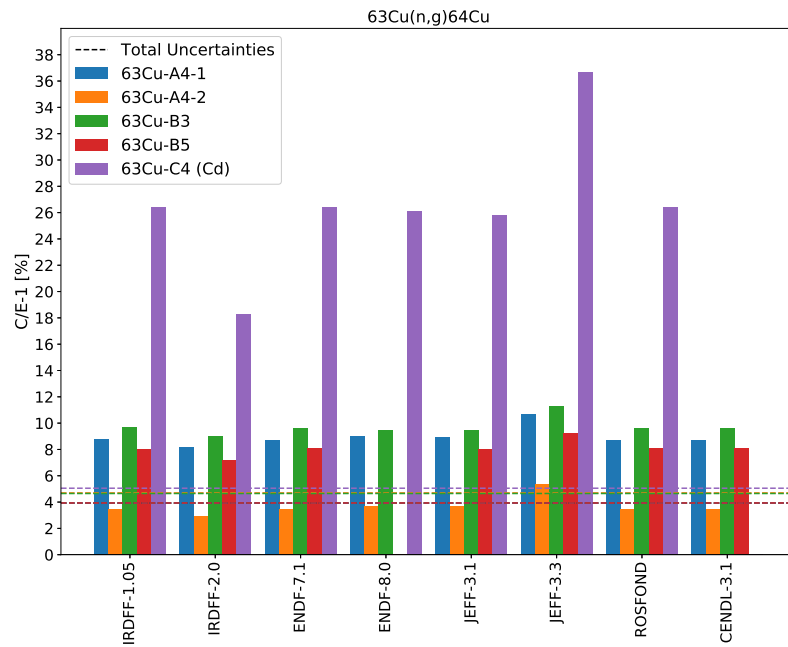


Figure 4.7: Reaction rates evaluation for $^{63}\text{Cu}(n,\gamma)^{64}\text{Cu}$.

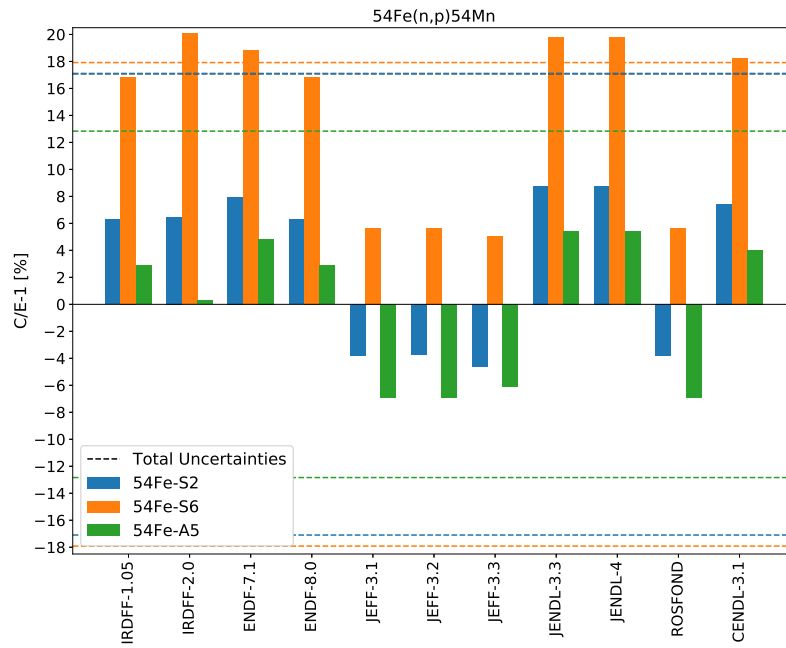


Figure 4.8: Reaction rates evaluation for $^{54}\text{Fe}(n,p)^{54}\text{Mn}$.

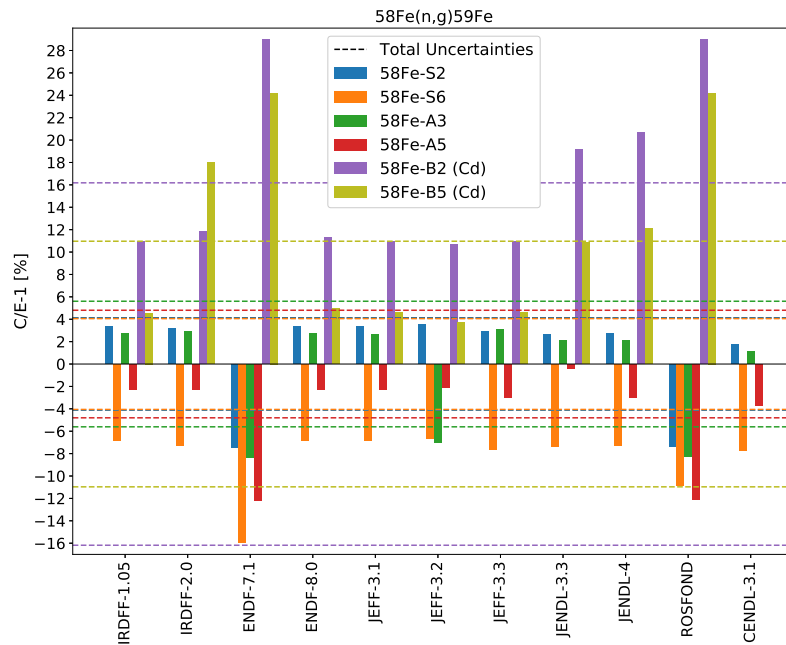


Figure 4.9: Reaction rates evaluation for $^{58}\text{Fe}(n,\gamma)^{59}\text{Fe}$.

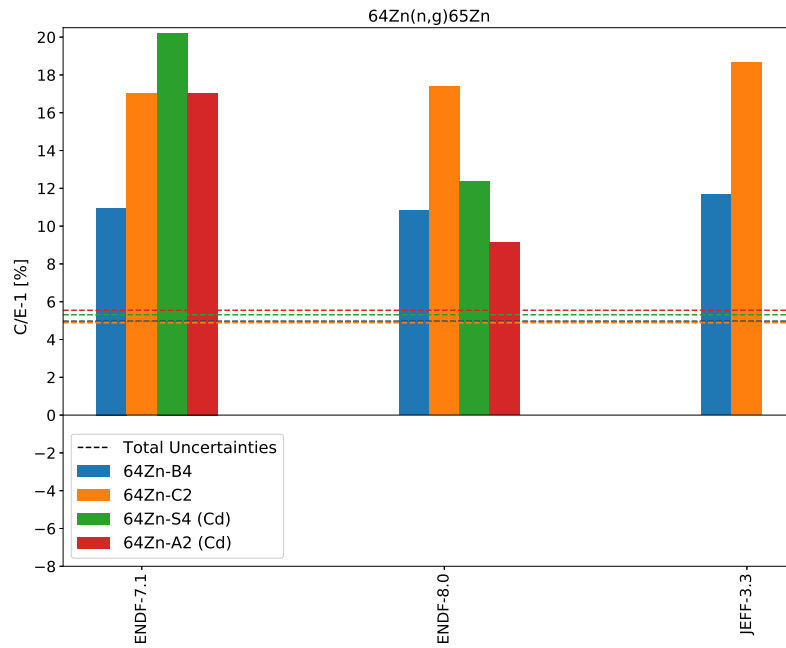


Figure 4.10: Reaction rates evaluation for $^{64}\text{Zn}(n,\gamma)^{65}\text{Zn}$.

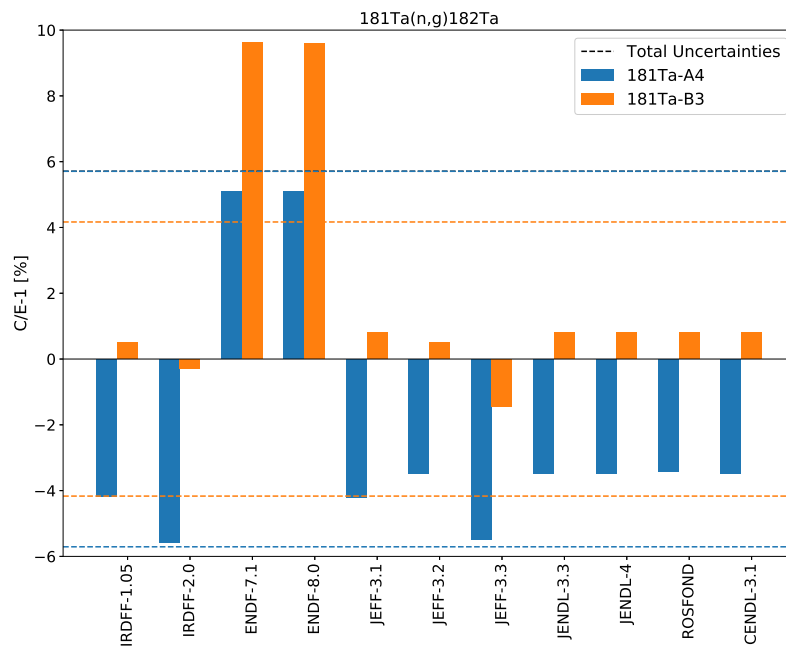


Figure 4.11: Reaction rates evaluation for $^{181}\text{Ta}(n,\gamma)^{182}\text{Ta}$.

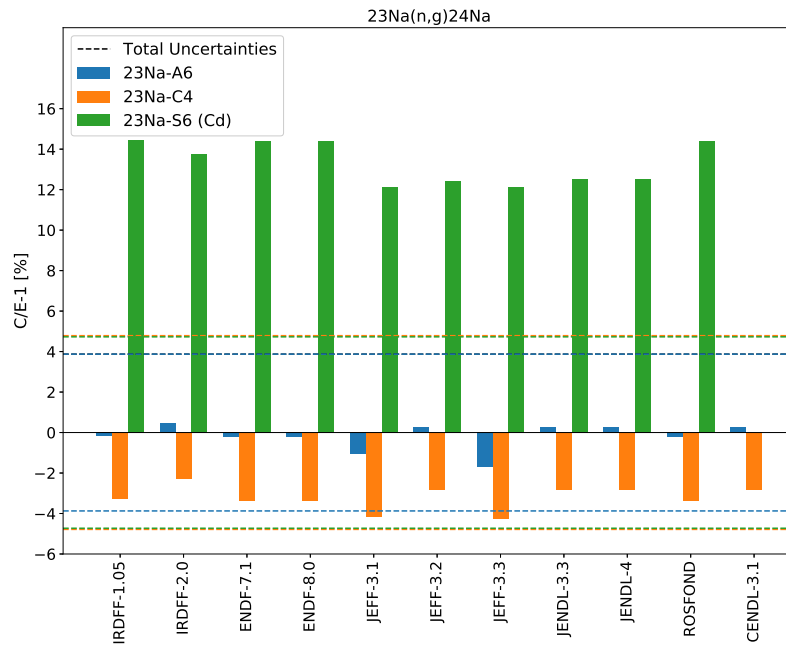


Figure 4.12: Reaction rates evaluation for $^{23}\text{Na}(n,\gamma)^{24}\text{Na}$.

4.3.1 Uncertainties

The overview of main uncertainties common for all the activation samples are given in Table 4.5. Besides included, other identified uncertainties such as the radionuclide half-life value uncertainty, the monitoring and measured foil geometrical position uncertainty, reactor shut-down time uncertainty, were considered as negligible in comparison with the count rate uncertainties. Statistical errors of the peaks measurements are followed in Table 4.6. Reaction rates and an activation are decreased by using Cd filter that led to the increased errors.

Table 4.5: Uncertainties common for all the activation samples.

Name of uncertainty	Value [%]
Statistical HPGe efficiency (averaged)	0.45
HPGe efficiency calibration	1.80
Measurement geometry	0.50
Coincidence summing factor (statistical, averaged)	0.45
Scaling factor (1st exp.)	2.81
Scaling factor (2nd exp.)	3.83
Statistical calculational (averaged, except $^{54}\text{Fe}(n,p)$)	0.40
Statistical calculational (averaged, $^{54}\text{Fe}(n,p)$)	2.00
MCNP core model	1.50
Holder geometry	0.10

Table 4.6: Statistical errors of the peaks measurements.

Reaction-position	Value [%]	Reaction-position	Value [%]
$^{63}\text{Cu}(n,\gamma)\text{-A4-1}$	1.02	$^{58}\text{Fe}(n,\gamma)\text{-A3}$	2.61
$^{63}\text{Cu}(n,\gamma)\text{-A4-2}$	0.96	$^{58}\text{Fe}(n,\gamma)\text{-A5}$	1.26
$^{63}\text{Cu}(n,\gamma)\text{-B3}$	0.74	$^{58}\text{Fe}(n,\gamma)\text{-B2 (Cd)}$	12.80
$^{63}\text{Cu}(n,\gamma)\text{-B5}$	1.05	$^{58}\text{Fe}(n,\gamma)\text{-B5 (Cd)}$	5.81
$^{63}\text{Cu}(n,\gamma)\text{-C4 (Cd)}$	1.46	$^{181}\text{Ta}(n,\gamma)\text{-A4}$	0.89
$^{54}\text{Fe}(n,p)\text{-S2}$	16.68	$^{181}\text{Ta}(n,\gamma)\text{-B3}$	1.17
$^{54}\text{Fe}(n,p)\text{-S6}$	17.52	$^{23}\text{Na}(n,\gamma)\text{-A6}$	0.99
$^{54}\text{Fe}(n,p)\text{-A5}$	11.99	$^{23}\text{Na}(n,\gamma)\text{-C4}$	0.98
$^{58}\text{Fe}(n,\gamma)\text{-S2}$	1.37	$^{23}\text{Na}(n,\gamma)\text{-S6 (Cd)}$	1.08
$^{58}\text{Fe}(n,\gamma)\text{-S6}$	1.40		

Conclusion

The characterization of the neutron field in the graphite insertion of the LR-0 core was successfully made. Two neutron activation experiments were carried out. The characterization was provided by means of reaction rates evaluation for three well-validated reactions: $^{197}\text{Au}(n,\gamma)$, $^{58}\text{Ni}(n,p)$, $^{181}\text{Ta}(n,\gamma)$. The good agreement was achieved for all of them. The measured reaction rates of Ta agree with most libraries, besides ENDF/B libraries that overpredict the experiment. The similar agreements were appeared in the reference LR-0 neutron field. Based on the valid characterization, cross-sections of dosimetric reactions were evaluated. The Cd filter was used to test cross-sections in the resonance energy region. There were $^{63}\text{Cu}(n,\gamma)$, $^{54}\text{Fe}(n,p)$, $^{58}\text{Fe}(n,\gamma)$, $^{23}\text{Na}(n,\gamma)$, $^{64}\text{Zn}(n,\gamma)$ reactions. The evaluation of reaction rates was made based on the methods and theory studied in the work. Monte Carlo models of HPGe detector and the reactor were used to determine reaction rates in different nuclear data libraries, and to calculate the neutron spectrum in the graphite insertion. The effect of neutron filters in the issue of cross-sections validation was showed. The uncertainties estimation of obtained reaction rates was made as well.

In the case of $^{58}\text{Fe}(n,\gamma)$, most of libraries are in satisfactory agreement with the experiment, while ENDF/B-VII.1 and ROSFOND-2010 underpredict experimental results for bare samples and overpredict for Cd covered samples. For $^{54}\text{Fe}(n,p)$, all the libraries predict experiment well and within uncertainties. However, there are high statistics uncertainty of the peak measurements that makes it hard to evaluate correctly. Results of $^{63}\text{Cu}(n,\gamma)$ and $^{64}\text{Zn}(n,\gamma)$ reactions show that libraries overpredict experiment by about 8% and 15% for bare samples, and by about 26% and 12 % for samples in Cd, respectively. The results for $^{23}\text{Na}(n,\gamma)$ indicated that the calculations for bare samples are in a good agreement for all the libraries. For the reaction in Cd, it was showed that all the libraries overpredict experimental results by about 13%. Based on that, it can be estimated that there are some inaccuracies in reaction resonance cross-section. By this case, the specific importance of using neutron filters to test cross-sections in different energy region is indicated evidently.

The topic of reaction rates (and spectrum averaged cross-sections) evaluation was studied in the work. The issue of validation is significant in the neutron reactions problems. Using the

LR-0 modular design and well-described evaluation methods, many more experiments on LR-0 can be carried out to solve the wide range of cross-sections validation tasks.

Bibliography

- [1] Nicola Burianová. Cross section measurement in reactor spectrum: ^{55}Mn (n, 2n), ^{90}Zr (n, 2n), ^{127}I (n, 2n), master's thesis, univerzita karlova, matematicko-fyzikální fakulta. 2018.
- [2] Nicola Burianová, Martin Schulc, Jan Šimon, Martin Mareček, Jan Uhlíř, et al. Measurement of selected differential cross sections in ^{235}U spectrum. *Journal of Nuclear Engineering and Radiation Science*, 5(3), 2019.
- [3] M. Drog. Monoenergetic neutron production by two-body reactions in the energy range from 0.0001 to 500 mev. In *An overview. TCM-Meeting of IAEA, Debrecen, Hungary*, 1999.
- [4] P. Dryák and P. Kovář. Experimental and mc determination of hpge detector efficiency in the 40–2754 kev energy range for measuring point source geometry with the source-to-detector distance of 25 cm. *Applied Radiation and Isotopes*, 64(10-11):1346–1349, 2006.
- [5] P. Dryák, J. Šolc, and P. Kovář. Correction of the true summations in volume sources. *Applied Radiation and Isotopes*, 70(9):2130–2132, 2012.
- [6] U. Farinelli. Nuclear data and integral experiments in reactor physics. Technical report, 1980.
- [7] S. Geelen. Study of parameters influencing the response of hpge-detectors. Master's thesis, UHasselt, 2018.
- [8] T. Goorley, M. James, Thomas Booth, F. Brown, J. Bull, L.J. Cox, J. Durkee, J. Elson, Michael Fensin, RA. Forster, et al. Initial mcnp6 release overview. *Nuclear Technology*, 180(3):298–315, 2012.
- [9] Patrick J Griffin and JG Kelly. A rigorous treatment of self-shielding and covers in neutron spectra determinations. *IEEE Transactions on Nuclear Science*, 42(6):1878–1885, 1995.

- [10] S. Kafala. Simple method for true coincidence summing correction. *Journal of radioanalytical and nuclear chemistry*, 191(1):105–114, 1995.
- [11] R. Kinsey. National nuclear data center. *Nuclear Data from Nubat at Brookhaven National*, 1979.
- [12] GF. Knoll. Radiation detection and measurement 3rd edition John Wiley and Sons. *New York*, 2000.
- [13] Michal Košťál, Vojtěch Rypar, Martin Schulc, Evžen Losa, Petr Baroň, Martin Mareček, and Jan Uhlíř. Measurement of ^{75}As (n, 2n) cross section in well-defined spectrum of Ir-0 special core. *Annals of Nuclear Energy*, 100:42–49, 2017.
- [14] Michal Košťál, Martin Schulc, Jaroslav Šoltés, Evžen Losa, Ladislav Viererbl, Zdeněk Matěj, František Cvachovec, and Vojtěch Rypar. Measurements of neutron transport of well defined silicon filtered beam in lead. *Applied Radiation and Isotopes*, 142:160–166, 2018.
- [15] M. Košťál, Z. Matěj, F. Cvachovec, V. Rypar, E. Losa, J. Rejchrt, F. Mravec, and M. Veškrna. Measurement and calculation of fast neutron and gamma spectra in well defined cores in Ir-0 reactor. *Applied Radiation and Isotopes*, 120:45–50, 2017.
- [16] M. Košťál, Z. Matěj, E. Losa, O. Huml, M. Štefánik, F. Cvachovec, M. Schulc, B. Jánský, E. Novák, D. Harutyunyan, and V. Rypar. On similarity of various reactor spectra and ^{235}U prompt fission neutron spectrum. *Applied Radiation and Isotopes*, 135:83–91, 2018.
- [17] M. Košťál, V. Rypar, J. Milčák, V. Juříček, E. Losa, B. Forget, and S. Harper. Study of graphite reactivity worth on well-defined cores assembled on Ir-0 reactor. *Annals of Nuclear Energy*, 87:601–611, 2016.
- [18] M. Košťál, M. Schulc, V. Rypar, E. Losa, N. Burianová, J. Šimon, M. Mareček, and J. Uhlíř. Validation of zirconium isotopes (n,g) and (n,2n) cross sections in a comprehensive Ir-0 reactor operative parameters set. *Applied Radiation and Isotopes*, 128:92–100, 2017.
- [19] M. Košťál, M. Veškrna, F. Cvachovec, B. Jánský, E. Novák, V. Rypar, J. Milčák, E. Losa, F. Mravec, Z. Matěj, J. Rejchrt, B. Forget, and S. Harper. Comparison of fast neutron spectra in graphite and FLiNa salt inserted in well-defined core assembled in Ir-0 reactor. *Annals of Nuclear Energy*, 83:216–225, 2015.

- [20] M. Košťál, M. Švadlenková, P. Baroň, V. Rypar, and J. Milčák. Determining the axial power profile of partly flooded fuel in a compact core assembled in reactor Ir-0. *Annals of Nuclear Energy*, 90:450–458, 2016.
- [21] M. Košťál, M. Schulc, J. Šimon, N. Burianová, D. Harutyunyan, E. Losa, and V. Rypar. Measurement of various monitors reaction rate in a special core at Ir-0 reactor. *Annals of Nuclear Energy*, 112:759–768, 2018.
- [22] Jaakko Leppänen, Maria Pusa, Tuomas Viitanen, Ville Valtavirta, and Toni Kaltiaisenaho. The serpent monte carlo code: Status, development and applications in 2013. *Annals of Nuclear Energy*, 82:142–150, 2015.
- [23] W. Mannhart. Evaluation of the cf-252 fission neutron spectrum between 0 mev and 20 mev. In *Properties of Neutron Sources*, pages 158–171. Citeseer, 1987.
- [24] Customization Tools Manual. Canberra spectroscopy software genie-2000, 2004.
- [25] Nuclear Power contributors. nuclear-power.net - neutron cross-section [online]. <https://www.nuclear-power.net/neutron-cross-section/>.
- [26] T. Peltan, M. Košťál, J. Prehradný, M. Schulc, and V. Dostál. Validation of graphite cross section in various integral experiments. 2019.
- [27] J.J. Powers, N.R. Brown, D.E. Mueller, B.W. Patton, E. Losa, and M. Košťál. Sensitivity/uncertainty analyses comparing Ir-0 reactor experiments containing flibe salt with models for molten-salt-cooled and molten-salt-fueled reactors. *Annals of Nuclear Energy*, 120:319–332, 2018.
- [28] V. Radulovic and A. Trkov. Integral data in nuclear data evaluation, indc(nds)-0746. Technical report, INDC International Nuclear Data Committee, IAEA Nuclear Data Section, 2017.
- [29] Martin Ruščák, Otakar Frýbort, David Harut, Martin Mareček, Guido Mazzini, Josef Pilát, and Marek Ruščák. Energy well: Conceptual design of a small molten salt cooled reactor as an opportunity for the czech industry. *Bezpečnost Jaderne Energie*, 26(5-6):120–135, 2018.
- [30] Jakub Rychlecký. Research reactor Ir-0 [online]. <http://cvrez.cz/en/infrastructure/research-reactor-ir-0/>.

- [31] M. Schulc, M. Košťál, R. Capote, E. Novák, J. Šimon, N. Burianová, and A. Wallner. Validation of selected (n,2n) dosimetry reactions in irdff-1.05 library. *Applied Radiation and Isotopes*, 143:132–140, 2019.
- [32] M. Schulc, M. Košťál, E. Novák, and T. Czako. Validation of nickel isotopes neutron cross sections using nickel spherical benchmark. *Applied Radiation and Isotopes*, 140:247–251, 2018.
- [33] M. Schulc, M. Košťál, J. Šimon, E. Novák, M. Mareček, and R. Kubín. Validation of irdff-ii library by means of 252cf spectral averaged cross sections. *Applied Radiation and Isotopes*, 155, 2020.
- [34] E. Tomarchio and S. Rizzo. Coincidence-summing correction equations in gamma-ray spectrometry with p-type hpgedetectors. *Radiation Physics and Chemistry*, 80(3):318–323, 2011.
- [35] Peltan Tomáš. Ověření materiálového parametru reaktoru typu htgr. Master's thesis, CTU in Prague, 2019.
- [36] Andrej Trkov, Patrick J Griffin, SP Simakov, Lawrence R Greenwood, Konstantin I Zolotarev, Roberto Capote, Daniel L Aldama, V Chechev, Christophe Destouches, AC Kahler, et al. IRDFF-II: A New Neutron Metrology Library. *Nuclear Data Sheets*, 163:1–108, 2020.
- [37] Andrej Trkov, Gašper Žerovnik, Luka Snoj, and Matjaž Ravnik. On the self-shielding factors in neutron activation analysis. *Nuclear Instruments and Methods in Physics Research Section A: Accelerators, Spectrometers, Detectors and Associated Equipment*, 610(2):553–565, 2009.
- [38] Jana Ulmanová. Studium vlivu ocelového reflektoru na kritičnost. Master's thesis, CTU in Prague, 2019.
- [39] Tim Vidmar, Matjaž Korun, and Branko Vodenik. A method for calculation of true coincidence summing correction factors for extended sources. *Applied radiation and isotopes*, 65(2):243–246, 2007.
- [40] John G Williams, David W Vehar, Frank H Ruddy, and David M Gilliam. *Reactor Dosimetry: Radiation Metrology and Assessment*, volume 1398. ASTM International, 2001.

- [41] Gašper Žerovnik, Manca Podvratnik, and Luka Snoj. On normalization of fluxes and reaction rates in mcnp criticality calculations. *Annals of Nuclear Energy*, 63:126–128, 2014.
- [42] Willem Lambert Zijp, Henk J Nolthenius, and Geert CHM Verhaag. Cross-section library doscros84 (in a 640 group structure of the sand-ii type). Technical report, Netherlands Energy Research Foundation, 1984.

Appendix A

Comparison of Reaction Rates

Table A.1: Comparison of reaction rates for $^{63}\text{Cu}(n,\gamma)^{64}\text{Cu}$.

Position	A4-1	A4-2	B3	B5	C4 (Cd)
$q_{exp} [s^{-1}]$	1.705E-28	1.791E-28	1.690E-28	1.667E-28	1.351E-29
Tot. uncertainty	3.92	4.70	4.65	3.93	5.05
Library	C/E-1 [%]				
IRDF-1.05	8.76	3.49	9.66	8.04	26.40
IRDF-2.0	8.15	2.91	9.01	7.22	18.27
ENDF-7.1	8.71	3.44	9.61	8.09	26.40
ENDF-8.0	8.98	3.69	9.48	8.09	26.12
JEFF-3.1	8.95	3.67	9.46	8.02	25.81
JEFF-3.3	10.70	5.33	11.30	9.21	36.70
ROSFOND	8.71	3.43	9.61	8.09	26.40
CENDL-3.1	8.71	3.44	9.61	8.10	–

Table A.2: Comparison of reaction rates for $^{64}\text{Zn}(n,\gamma)^{65}\text{Zn}$.

Position	B4	C2	S4 (Cd)	A2 (Cd)
$q_{exp} [s^{-1}]$	3.104E-29	2.763E-29	4.047E-30	3.408E-30
Tot. uncertainty	4.96	4.89	5.31	5.55
Library	C/E-1 [%]			
ENDF-7.1	10.95	17.03	20.22	17.04
ENDF-8.0	10.81	17.39	12.37	9.12
JEFF-3.3	11.65	18.65	–	–

Table A.3: Comparison of reaction rates for $^{54}\text{Fe}(n,p)^{54}\text{Mn}$.

Position	S2	S6	A5
$q_{exp} [s^{-1}]$	2.920E-31	2.835E-31	3.371E-31
Tot. uncertainty	17.10	17.92	12.84
Library	C/E-1 [%]		
IRDF-1.05	6.29	16.87	2.88
IRDF-2.0	6.50	20.06	0.29
ENDF-7.1	7.97	18.82	4.83
ENDF-8.0	6.29	16.87	2.88
JEFF-3.1	-3.79	5.65	-6.92
JEFF-3.2	-3.78	5.67	-6.91
JEFF-3.3	-4.60	5.05	-6.08
JENDL-3.3	8.78	19.77	5.44
JENDL-4	8.78	19.77	5.44
ROSFOND	-3.79	5.65	-6.92
CENDL-3.1	7.43	18.24	4.01

Table A.4: Comparison of reaction rates for $^{58}\text{Fe}(n,\gamma)^{59}\text{Fe}$.

Position	S2	S6	A3	A5	B2 (Cd)	B5 (Cd)
$q_{exp} [s^{-1}]$	4.987E-29	5.184E-29	5.201E-29	5.330E-29	3.031E-30	3.601E-30
Tot. uncertainty	4.07	4.06	5.61	4.80	16.18	10.97
Library	C/E-1 [%]					
IRDF-1.05	3.37	-6.85	2.69	-2.30	10.91	4.56
IRDF-2.0	3.17	-7.31	2.95	-2.27	11.83	18.02
ENDF-7.1	-7.43	-15.90	-8.37	-12.21	28.94	24.21
ENDF-8.0	3.38	-6.84	2.70	-2.29	11.32	4.93
JEFF-3.1	3.36	-6.87	2.67	-2.32	10.90	4.58
JEFF-3.2	3.55	-6.68	-6.99	-2.14	10.69	3.71
JEFF-3.3	2.93	-7.66	3.07	-3.00	10.91	4.58
JENDL-3.3	2.65	-7.40	2.11	-0.37	19.19	10.88
JENDL-4	2.75	-7.26	2.07	-2.96	20.64	12.12
ROSFOND	-7.32	-10.85	-8.25	-12.11	28.94	24.21
CENDL-3.1	1.75	-7.72	1.14	-3.70	–	–

Table A.5: Comparison of reaction rates for $^{181}\text{Ta}(n,\gamma)^{182}\text{Ta}$.

Position	A4	B3
$q_{exp} [s^{-1}]$	2.972E-27	2.706E-27
Tot. uncertainty	5.71	4.17
Library	C/E-1 [%]	
IRDF-1.05	-4.19	0.51
IRDF-2.0	-5.58	-0.28
ENDF-7.1	5.09	9.61
ENDF-8.0	5.08	9.61
JEFF-3.1	-4.21	0.80
JEFF-3.2	-3.48	0.50
JEFF-3.3	-5.50	-1.43
JENDL-3.3	-3.48	0.80
JENDL-4	-3.48	0.79
ROSFOND	-3.43	0.82
CENDL-3.1	-3.47	0.81

Table A.6: Comparison of reaction rates for $^{23}\text{Na}(n,\gamma)^{24}\text{Na}$.

Position	A6	C4	S6 (Cd)
$q_{exp} [s^{-1}]$	1.888E-29	2.173E-29	9.049E-31
Tot. uncertainty	4.73	3.87	4.73
Library	C/E-1 [%]		
IRDF-1.05	-0.17	-3.30	14.44
IRDF-2.0	0.47	-2.27	13.75
ENDF-7.1	-0.23	-3.36	14.40
ENDF-8.0	-0.23	-3.36	14.40
JEFF-3.1	-1.07	-4.18	12.14
JEFF-3.2	0.28	-2.85	12.44
JEFF-3.3	-1.69	-4.27	12.14
JENDL-3.3	0.29	-2.84	12.52
JENDL-4	0.29	-2.84	12.52
ROSFOND	-0.23	-3.36	14.40
CENDL-3.1	0.28	-2.85	0.00